

Bine Trees: Enhancing Collective Operations by Optimizing Communication Locality

Daniele De Sensi
Sapienza University of Rome
Rome, Italy
desensi@di.uniroma1.it

Saverio Pasqualoni
Sapienza University of Rome
Rome, Italy
pasqualoni.1845572@studenti.uniroma1.it

Lorenzo Piarulli
Sapienza University of Rome
Rome, Italy
piarulli@di.uniroma1.it

Tommaso Bonato
ETH Zurich
Zurich, Switzerland
tommaso.bonato@inf.ethz.ch

Seydou Ba
RIKEN
Kobe, Japan
seydou.ba@riken.jp

Matteo Turisini
CINECA
Rome, Italy
m.turisini@cineca.it

Jens Domke
RIKEN
Kobe, Japan
jens.domke@riken.jp

Torsten Hoefler
ETH Zurich
Zurich, Switzerland
torsten.hoefler@inf.ethz.ch

Abstract

Communication locality plays a key role in the performance of collective operations on large HPC systems, especially on oversubscribed networks where groups of nodes are fully connected internally but sparsely linked through global connections. We present *Bine* (*binomial negabinary*) trees, a family of collective algorithms that improve communication locality. *Bine* trees maintain the generality of binomial trees and butterflies while cutting global-link traffic by up to 33%. We implement eight *Bine*-based collectives and evaluate them on four large-scale supercomputers with Dragonfly, Dragonfly+, oversubscribed fat-tree, and torus topologies, achieving up to 5× speedups and consistent reductions in global-link traffic across different vector sizes and node counts.

CCS Concepts

• Computing methodologies → Distributed algorithms; • Networks → Data center networks.

Keywords

collective communication, topology, binomial tree, MPI, NCCL

ACM Reference Format:

Daniele De Sensi, Saverio Pasqualoni, Lorenzo Piarulli, Tommaso Bonato, Seydou Ba, Matteo Turisini, Jens Domke, and Torsten Hoefler. 2025. Bine Trees: Enhancing Collective Operations by Optimizing Communication Locality. In *The International Conference for High Performance Computing, Networking, Storage and Analysis (SC '25)*, November 16–21, 2025, St Louis, MO, USA. ACM, New York, NY, USA, 18 pages. <https://doi.org/10.1145/3712285.3759835>

1 Introduction

As high-performance computing (HPC) systems and data centers continue to grow [1, 5, 41, 42], communication locality plays a crucial role in determining performance. In most HPC networks, communication with nearby nodes is generally faster than with distant nodes. This is particularly evident in scale-up networks, where bandwidth can be up to an order of magnitude higher than that of the scale-out network [20, 30]. However, even when focusing solely on the scale-out network, locality remains important. While full-bandwidth scale-out networks such as fat trees can deliver high performance, they also come with significant cost and power consumption. As a result, *oversubscribed* (*tapered*) networks are often used. These are typically organized into fully connected *groups*, such as groups in Dragonfly/Dragonfly+ topologies [6, 19, 36, 58] or subtrees in oversubscribed fat trees, which are then interconnected more sparsely through *global links*.

Reducing the traffic forwarded over global links is advantageous for several reasons. First, global links are often longer than local links, resulting in higher communication latency [6, 19]. Second, because global links are typically oversubscribed, they can sustain only a limited number of concurrent communications, often causing congestion when multiple ranks from the same or different applications contend for the same link, leading to higher latency and lower throughput [14, 18, 20, 59]. This issue is amplified in oversubscribed low-diameter networks, where jobs are usually distributed across multiple groups. Such distribution helps arbitrary traffic patterns approximate uniform behavior, under which these topologies achieve high throughput [11, 34, 56, 63, 65], but it also increases global link utilization. Third, global links consume more energy than local links, making it crucial to reduce their usage [2]. Last, as the physical size of data centers and supercomputers approaches practical limits, tightly coupled applications run across multiple geographically distributed data centers [12, 21, 26, 38, 52]. In such scenarios, communication between distinct data centers or supercomputers must traverse even slower Wide-Area Network (WAN) links, and improving communication locality is critical.



This work is licensed under a Creative Commons Attribution 4.0 International License. SC '25, St Louis, MO, USA

© 2025 Copyright held by the owner/author(s).
ACM ISBN 979-8-4007-1466-5/2025/11
<https://doi.org/10.1145/3712285.3759835>

For these reasons, running collectives on oversubscribed networks requires careful scheduling of communications to minimize traffic on global links and ensure scalability. Consider, for example, a broadcast operation implemented with a binomial tree. The root first sends the data to one process, and then each process forwards it to another, doubling the number of participants at each step until all processes have received the data. The algorithm remains correct as long as each process that has received the data sends it to one that has not, but different choices of destination processes can result in different amounts of traffic on global links.

For instance, consider the scenario in Fig. 1, where eight nodes are connected through a 2:1 oversubscribed fat-tree. Each leaf switch has two downlinks and one uplink, serving two nodes per switch. In a *distance-doubling* binomial tree (as in Open MPI [43, 44], top part of Fig. 1), the distance between communicating ranks doubles at each step (e.g., rank 0 first sends its data to rank 1, then to rank 2). In contrast, in a *distance-halving* tree (as in MPICH [48], bottom part of the Fig. 1), the distance halves at each step (e.g., rank 0 first sends its data to rank 4, then to rank 2). In both cases, each rank that has already received the n bytes of the vector forwards them to another rank. The distance-doubling broadcast forwards a total of $6n$ bytes over global links ($2n$ at step 1 and $4n$ at step 2), compared to only $3n$ bytes for the distance-halving variant.

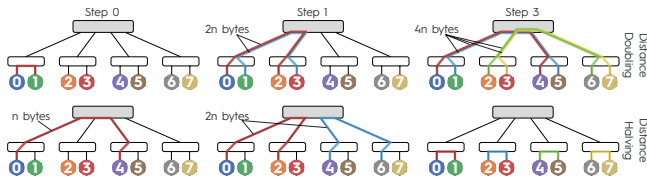


Figure 1: Traffic on global links for a broadcast collective using *distance-doubling* and *distance-halving* binomial trees.

This shows that, despite both algorithms requiring the same number of steps and transferring the same total data volume, the distance-halving variant is more efficient in reducing global link usage. Intuitively, closer communication is preferable when more ranks are involved in sending data. Furthermore, if all links offer the same bandwidth, having two data transfers sharing a link can halve the effective injection bandwidth, as in step 1 of distance-doubling, between ranks 0-2 and 1-3. Though simplified for illustrative purposes, this example shows how the communication schedule affects inter-group traffic and performance.

Moreover, although ring algorithms reduce global link traffic compared to binomial trees and butterflies, their performance is suboptimal for large numbers of ranks and/or small to medium vector sizes [17]. Also, it is important to note that existing hierarchical and locality-aware collective algorithms may not always be effective. These algorithms typically require prior knowledge of the number of processes per group and often assume that jobs run with the same number of processes in each group [10, 27, 33, 35, 61]. While such assumptions are reasonable for the number of processes per node, they may not hold when considering the partitioning of processes across subtrees or Dragonfly groups. In fact, the scheduler’s process-to-node allocation is not known in advance and is unlikely to result in an even distribution of processes across groups.

Based on these insights, this paper contributes as follows:

- We introduce *Bine* (*binomial negabinary*) trees¹, a novel way of constructing binomial trees (and butterflies) collective algorithms, reducing the distance between communicating processes and, consequently, the volume of data transmitted across groups (Sec. 2-3). *Bine* trees are topology-agnostic and generic as binomial trees and butterflies, but additionally optimize communication locality. They are orthogonal to hierarchical algorithms and can be used in both hierarchical and flat algorithms.
- We design and implement new collective algorithms based on *Bine* trees and butterflies for allgather, allreduce, reduce-scatter, alltoall, broadcast, gather, reduce, scatter (Sec. 4)².
- We evaluate *Bine* collectives on up to 8,192 nodes (Sec. 5), on four supercomputers with diverse network topologies: LUMI (Dragonfly), Leonardo (Dragonfly+), MareNostrum 5 (2:1 oversubscribed fat-tree), and Fugaku (torus). We include three different MPI implementations: Fujitsu MPI, Open MPI, and Cray MPICH, as well as NCCL. *Bine* trees consistently outperform state-of-the-art algorithms, improving performance by up to 80% on LUMI and MareNostrum 5, 50% on Leonardo, and up to 5× on Fugaku, while also reducing global link load by up to 33%. These results demonstrate the effectiveness of *Bine* trees in optimizing collective communication, delivering substantial performance and scalability benefits across diverse networks and software stacks.

2 Distance-Halving *Bine* Trees

We now recall the construction of binomial trees (Sec. 2.1), then introduce distance-halving *Bine* trees visually (Sec. 2.2) and formally (Sec. 2.3), and discuss their advantages over binomial trees (Sec. 2.4).

2.1 Binomial Trees Construction

As shown in Fig. 2, a distance-halving binomial tree of order 0 consists of a single node. A tree of order k is built recursively by linking two trees of order $k - 1$, making one the child of the other. When used in collective operations, each node maps to a rank, and each edge represents communication between ranks. Any mapping of ranks to nodes yields a valid algorithm, also for collectives involving computation (e.g., reduce), as long as the operator is associative, which MPI assumes by default.

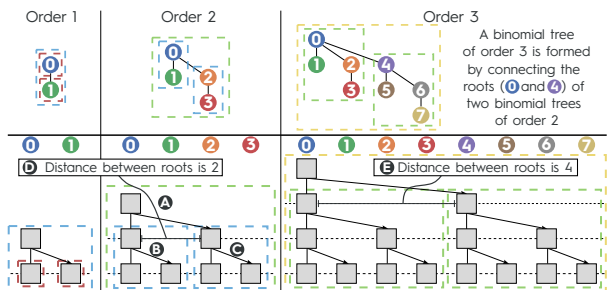


Figure 2: Distance-halving binomial tree construction.

Although the view of binomial trees shown in the top part of Fig. 2 highlights the recursive construction of the tree, it does not

¹A *bine* is a twisting vine, reminding the way in which we build *Bine* trees (Sec. 2.2).

²Reference implementations are available at <https://github.com/HLC-Lab/bine-trees>.

clearly illustrate how communication progresses step by step. To make this explicit, we use the representation in the bottom part of Fig. 2, where ranks are arranged left to right and each row (indicated with a dashed horizontal line) corresponds to a communication step. Boxes indicate that the value is present in a rank’s memory. Vertical lines show a rank lifetime, while diagonal arrows represent message transfers between ranks. For example, in a broadcast across four ranks (i.e., a tree of order 2) with rank 0 as root, rank 0 first sends the data to rank 2 (Fig. 2, **A**). In the next step, rank 0 sends the data to rank 1 (Fig. 2, **B**), while rank 2 sends it to rank 3 (Fig. 2, **C**).

2.2 Bine Trees Construction: Visual Intuition

The key idea of *Bine* trees is to arrange ranks in a binomial tree so that communicating ranks are closer than in standard binomial trees. Reducing this distance increases the likelihood that communication remains within the same group, thereby benefiting from higher bandwidth and lower latency. To keep the algorithm simple and generic, and not tied to any specific topology, standard binomial trees do not use the actual physical distance between nodes (e.g., obtained from their location [40]); instead, they determine distances based on the difference in rank identifiers.

For example, in distance-halving binomial trees, rank 6 first communicates with rank 4 (distance 2) and then with rank 7 (distance 1). This scheme reasonably approximates physical distance when ranks are mapped linearly across the system, which is often the case (e.g., under Slurm’s default *block* distribution [55]). If this is not the case, a remapping to a *block* distribution could be applied when the communicator is created, and the remapped rank identifiers used instead of the original ones. On the systems used in this work, for instance, hostnames are numbered consecutively across groups or subtrees, so it is sufficient to sort ranks by hostname.

Since our goal is to design an algorithm as simple and generic as standard binomial tree algorithms, we adopt a similar approach but use the *modulo distance* between rank identifiers. Namely, we consider the p ranks to be arranged in a circle $0, 1, \dots, p - 1$ and define the distance between two ranks r and q as the minimum distance along the circle, i.e., $d(r, q) = \min((r - q) \bmod p, (q - r) \bmod p)$. To motivate this choice, consider three ranks (0, 1, 2), each in a different group. Standard binomial trees would regard the distance between ranks 0 and 2 as larger than that between ranks 0 and 1, whereas in practice, both involve inter-group communication and should therefore be treated as equal. Modular distance achieves this. Of course, counterexamples exist where the standard distance is more accurate. However, as shown in Secs. 2.4.2 and 5, for jobs spanning multiple groups, as is often the case, modular distance provides a better approximation of the actual distance, enabling *Bine* trees to outperform standard binomial trees in most scenarios.

We construct a distance-halving *Bine* tree recursively. A two-node *Bine* tree (Fig. 3, order 1) is identical to a standard binomial tree. To build a four-node (i.e., order 2) *Bine* tree, we connect an order 1 *Bine* tree (Fig. 3, **B**), to a mirrored order 1 *Bine* tree (i.e., reflected on the vertical axis) and placed to its left (Fig. 3, **A**). The mirrored tree is placed to the left rather than to the right to keep a shorter modulo distance between the roots of the subtrees (one rather than two as in a binomial tree – see Fig. 2, **D**). Ranks are numbered left to right starting from the root, wrapping around

once the rightmost node of the tree is reached (e.g., on the 4-node tree, ranks 2 and 3 are those on the left of the root).

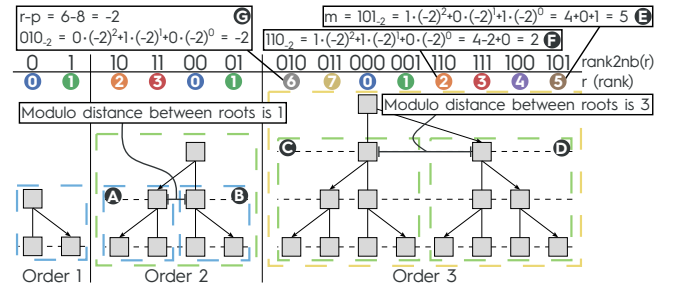


Figure 3: Distance-halving *Bine* trees construction.

The process generalizes recursively: an eight-node *Bine* tree is constructed by combining an order-2 *Bine* tree (Fig. 3, **C**) and a mirrored order-2 *Bine* tree (Fig. 3, **D**), placed side by side and arranged so that the modulo distance between the roots is as small as possible. In this case, placing the new four-node subtree on the right (rather than on the left) yields a root-to-root modulo distance of three, compared to five in the alternative placement. For comparison, the corresponding binomial tree would result in a modulo distance of four (Fig. 2, **E**). Appendix C discusses how to handle cases where the number of nodes is not a power of 2. Moreover, if the root is rank $t \neq 0$, we apply a logical rotation by subtracting t from all rank identifiers modulo p .

2.3 Bine Trees Construction: Formal Definition

We now provide a formal construction process for distance-halving *Bine* trees. Table 1 summarizes the notation we use.

Table 1: Notation used.

Symbol	Definition
p	Number of ranks.
r	Rank identifier.
s	Number of steps in a binomial or <i>Bine</i> tree collective ($s = \log_2 p$).
$rank2nb(r)$	Convert rank identifier r to its negabinary representation.
$nb2rank(r)$	Get rank identifier r from its negabinary representation.

2.3.1 Ranks Representation. In *Bine* trees, each rank is assigned a *negabinary* (i.e., negative-base) representation, where numbers are expressed as sums of powers of -2 instead of 2, as in standard binary. For example, the number 2 is represented as 110_{-2} , since $1 \cdot (-2)^2 + 1 \cdot (-2)^1 + 0 \cdot (-2)^0 = 4 - 2 = 2$. Unlike standard binary, negabinary representations can encode both positive and negative integers (e.g., $011_{-2} = -1$). As a result, there is no one-to-one correspondence between non-negative ranks and their negabinary representation. The largest positive number m that can be represented with a fixed number of negabinary bits is obtained by setting ones in all even positions and zeros in all odd positions. This ensures that only even powers of -2 , which contribute positive values, are included. For instance, on six bits $m = 010101_{-2} = 16 + 4 + 1 = 21$.

The construction of *Bine* trees ensures that the rightmost rank is m . For example, for a 8-nodes tree we need three bits, and $m =$

$101_{-2} = 5$ (Fig. 3, ㉑). Therefore, all ranks in the range $[0, m]$ (to the right of rank 0) can be represented using their positive negabinary value (e.g., Fig. 3, ㉒). Ranks greater than m (to the left of rank 0) are represented using the negabinary representation of $r - p$. For instance, rank $r = 6$ in an 8-node tree is represented as $6 - 8 = -2 = 010_{-2}$ (Fig. 3, ㉓).

We define the functions $rank2nb(r, p)$ and $nb2rank(r, p)$ to convert a rank identifier to its negabinary representation, and vice versa, for a collective on p ranks. For example, $rank2nb(2, 8) = 110_{-2}$ and $rank2nb(6, 8) = 010_{-2}$. Both functions can be efficiently implemented using bit masking and an addition or subtraction. When the context is clear, we will omit the p parameter and the $_{-2}$ base.

2.3.2 Determining the Communication Partner. In the broadcast, each rank must determine when to join the tree, or in other words, at which step it will receive data from its parent. We denote by u the number of consecutive least significant bits that are equal to each other, starting from the least significant bit. E.g., for a 16-node *Bine* tree, $u = 3$ for 1000, and $u = 2$ for 1011. In a distance-halving *Bine* tree broadcast, rank r receives data at step $i = s - u$ (with $i \in [0, s - 1]$). As illustrated in Fig. 4 ㉑, for rank 8, we have $rank2nb(8) = 1000$, so it receives data at step $i = s - u = 4 - 3 = 1$.

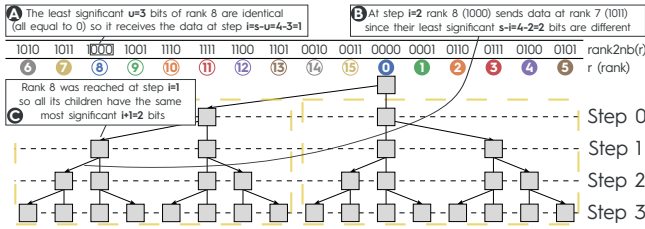


Figure 4: A 16-node (order 4) distance-halving *Bine* tree.

Once a rank receives the data, in each subsequent step i it forwards the data to rank:

$$q = nb2rank(rank2nb(r) \oplus \overbrace{111 \dots 1}^{s-i \text{ bits}}) \quad (1)$$

with \oplus denoting the XOR operation. In other words, at step i , each rank r that has already received the data will send it to a rank q whose negabinary representation differs in the least significant $s - i$ bits. For example, as shown in Fig. 4 ㉒, at step $i = 2$, rank 8 sends data at rank 7 since their negabinary representations (1000 and 1011, respectively), differ for the least significant $s - i = 4 - 2$ bits. For clarity, the complete MPI code of the distance-halving *Bine* tree algorithm for the broadcast is provided in Listing 1. Notably, the implementation is no more complex than that of standard binomial trees [43, 48]. Appendix C discusses how to handle cases where the number of nodes is not a power of 2.

Correctness can be easily demonstrated. For example, rank 4 receives the data via $0 \rightarrow 3 \rightarrow 4$, corresponding to the XOR combination $0000 \oplus 0111 \oplus 0011$. More generally, any s -bit number can be uniquely represented as the XOR of a subset of the binary/negabinary numbers $\{1, 11, 111, \dots, \underbrace{111 \dots 1}_s\}$, ensuring correctness.

```

1  int MPI_Bcast(void *buf, int count, MPI_Datatype dt, int root,
2              MPI_Comm comm){
3
4      int p, r;
5      MPI_Comm_size(comm, &p);
6      MPI_Comm_rank(comm, &r);
7      int recvd = (root == rank);
8      int vrank = mod(r - root, p);
9      int vrank_nb = rank2nb(vrank, p); // negabinary repr. of vrank
10     int mask = 0x1 << (int) log2(p) - 1; // mask with log2(p) LSBs set to 1
11     while(mask > 0){
12         int mask_lsbs = (mask << 1) - 1; // mask with s-i LSBs set to 1
13         int q = nb2rank(vrank_nb ^ mask_lsbs, p); // Eq. 1
14         q = mod(q + root, size); // Get the rank id
15         if(recvd){ // I send only if I already received the data
16             MPI_Send(buf, count, dt, q, 0, comm);
17         }else{
18             int lsbs = vrank_nb & mask_lsbs; // Get the s-i LSBs
19             if(!lsbs || lsbs == mask_lsbs){ // check if s-i LSBs all equal
20                 MPI_Recv(buf, count, dt, q, 0, comm, MPI_STATUS_IGNORE);
21                 recvd = 1;
22             }
23         }
24         mask >>= 1;
25     }
26     return MPI_SUCCESS;
    
```

Listing 1: *Bine* tree distance-halving broadcast code.

2.3.3 Determining Ranks in a Subtree. As we will discuss in Sec. 4, collectives like scatter (Sec. 4.2) require identifying all ranks in the subtree rooted at a given rank. After receiving data at step i , a rank applies XOR on its least significant bits to determine its next destination. This process recurses, and at each step, the $i + 1$ most significant bits remain unchanged. As a result, all descendants of a rank share the same $i + 1$ leading bits in their negabinary representation. For instance, in a 16-node *Bine* tree, rank 8 is reached at step $i = 1$, so all the ranks in the subtree rooted in 8 share its two most significant bits (i.e., 10, as shown in Fig. 4, ㉓).

2.4 Advantages over Binomial Trees

We know quantify the maximum reduction in global links traffic both theoretically (Sec. 2.4.1) and empirically (Sec. 2.4.2).

2.4.1 Theoretical Bound Computation. To explain why we expect *Bine* trees to reduce the number of bytes on global links compared to standard binomial trees, we start by considering the distance between communicating ranks. In standard distance-halving binomial trees, two communicating ranks differ for the bit in position $s - i - 1$ (i.e., the distance is $\delta_{binomial}(i) = 2^{s-i-1}$). In distance-halving *Bine* trees³, however, the negabinary representations of the two communicating ranks differ in the $s - i$ least significant bits, which are all equal to 1 for one rank, and all equal to 0 for the other rank. Thus, the distance between the two ranks at step i is: $\delta_{bine}(i) = |\sum_{j=0}^{s-i-1} (-2)^j| = |\frac{1}{3} - \frac{1}{3}(-2)^{s-i}| \approx \frac{2^{s-i}}{3}$.

In binomial trees, the maximum distance between ranks is $p/2$, so the distance between communicating ranks coincides with their modular distance. This allows us to compare *Bine* and standard binomial trees in terms of modular distance and to quantify the reduction in distance between communicating ranks using the ratio:

$$\frac{\delta_{bine}(i)}{\delta_{binomial}(i)} = \frac{2^{s-i}}{3 \cdot 2^{s-i-1}} = \frac{2}{3} \quad (2)$$

³Although we refer to it as a *distance-halving Bine* tree for simplicity, the distances do not halve exactly; instead, they differ by at most ± 1 from the ideal halving.

This implies that in *Bine* trees, communicating ranks are at a $\sim 33\%$ shorter modular distance compared to standard binomial trees, reducing the probability that communicating ranks are in different groups and communicate through global links.

Quantifying the exact reduction in inter-group traffic is challenging, as it heavily depends on the specific topology and on how ranks are allocated to groups. However, we can estimate an upper bound by considering a worst-case scenario in which each group only has a single outgoing link to another group. Let us focus on a specific step i and assume the group size equals $\delta_{binomial}(i)$, so that all communications in the standard binomial tree cross group boundaries. In this worst-case scenario, all $\delta_{binomial}(i)$ communications are directed to nodes in other groups, whereas for *Bine* trees this only happens for $\delta_{bine}(i)$ communications. Thus, the maximum reduction in global link traffic corresponds to the ratio $\delta_{bine}(i)/\delta_{binomial}(i)$, which, as shown in Eq. 2, is equal to $2/3$. In other words, *Bine* reduces by at most 33% the traffic on global links.

2.4.2 Empirical Analysis. We additionally validated our assumptions empirically by analyzing one-week job allocation data from the Leonardo [62] supercomputer and two-weeks data from the LUMI [22] supercomputer. Using Slurm commands (`queue` and `scontrol`), we obtained the list of jobs running on the system and, for each job, the hostnames of the allocated nodes. We then identified the Dragonfly/Dragonfly+ group to which each node was assigned. On Leonardo, we relied on existing hostname-to-group mappings [15], while on LUMI we extracted this information using the `sinfo -N -o "%N %f"` command. With this data, we determined the group assignment of each rank for every job. Based on this mapping we estimated, for each job, the global traffic of an allreduce operation using standard binomial and *Bine* trees, and computed the resulting traffic reduction achieved by *Bine* across allocations.

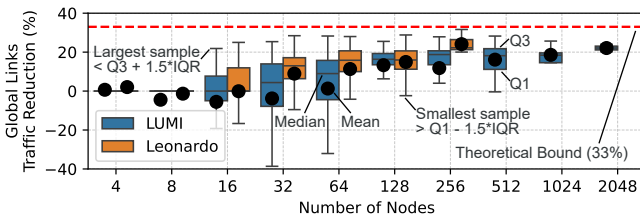


Figure 5: Reduction in global traffic on Leonardo and LUMI.

We present this analysis in Fig. 5, where we report the distribution of global traffic reduction across jobs using boxplots, grouped by the number of nodes. The data includes a total of 1,116 jobs on Leonardo and 1,914 jobs on LUMI. The largest observed jobs spanned up to 256 nodes on Leonardo and 2,048 nodes on LUMI, matching the maximum job sizes allowed on the two systems. For clarity, outliers are not shown in the figure. No outliers above the theoretical upper bound of 33% were observed, coherently with our model (Eq. 2). In a few cases, all occurring on less than 64 nodes, *Bine* trees increase global traffic. As discussed in Sec.2.2, this happens because *Bine* minimizes distance modulo p rather than the actual distance. In contrast, for larger allocations, *Bine* consistently outperforms standard binomial trees. The reduction in global link

traffic increases with the number of nodes, as larger jobs typically span more groups, creating more opportunities for *Bine* to reduce inter-group communication.

3 *Bine* Butterflies and Distance-Doubling Trees

3.1 *Bine* Butterflies

In a butterfly communication pattern, each rank exchanges data with another rank at every step. A *Bine* distance-halving butterfly can be seen as the superposition of multiple distance-halving *Bine* trees, each rooted at a different rank. The left part of Figure 6 illustrates this view, highlighting the trees rooted at ranks 2 and 3 with solid orange and dotted red lines, respectively.

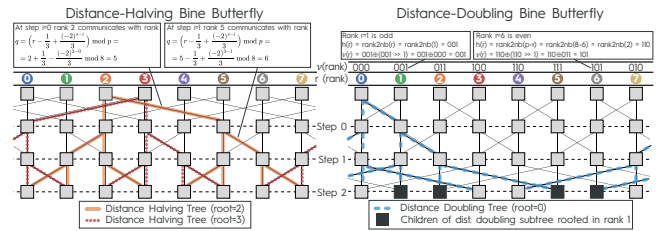


Figure 6: An 8-node distance-halving *Bine* butterfly (left), and distance-doubling *Bine* butterfly (right).

To guarantee correctness, these trees must be arranged so that the send and receive decisions are consistent across all ranks. We start from the distance-halving tree rooted in rank 0. As discussed in Sec. 2.3, at step i rank 0 communicates with a rank whose negabinary representation has the least significant $s - i$ bits set to 1, and the remaining bits set to 0, i.e., with rank:

$$q = \left(\sum_{j=0}^{s-i-1} (-2)^j \right) \bmod p = \left(\frac{1}{3} - \frac{(-2)^{s-i}}{3} \right) \bmod p \quad (3)$$

Even ranks r communicate as rank 0, but rotated to the right by r positions. Moreover, since each rank communicates with another one whose negabinary representation differs in the last $i + 1$ bits, even ranks always communicate with odd ranks, and vice versa. Consequently, odd ranks r communicate in a mirrored way with respect to the even rank $r - 1$. Thus, the communication partner q for a rank r at step i can be determined as:

$$q = \begin{cases} \left(r + \frac{1}{3} - \frac{(-2)^{s-i}}{3} \right) \bmod p & \text{if } r \text{ is even} \\ \left(r - \frac{1}{3} + \frac{(-2)^{s-i}}{3} \right) \bmod p & \text{if } r \text{ is odd} \end{cases} \quad (4)$$

Since the distance between communicating ranks in *Bine* butterflies matches that of *Bine* trees, distance-halving *Bine* butterflies reduce global traffic by up to 33% compared to standard distance-halving butterflies. Distance-halving butterflies are advantageous for collectives that increase the size of the exchanged data at each step, such as allgather, since in the last steps, where more data is transmitted, communication happens between closer nodes. Alternatively, it is possible to build a distance-doubling *Bine* butterfly by inverting the communication order, as shown in the right part of Fig. 6. This is preferable for collectives that exchange more data

in the first steps, such as reduce-scatter (Sec. 4.3). Appendix C discusses how to handle cases where the number of nodes is not a power of 2.

3.2 Distance-Doubling *Bine* Trees

We now describe the construction of distance-doubling *Bine* trees, using as a reference the one rooted in 0, shown with dashed blue lines in the right part of Fig. 6.

3.2.1 Ranks Representation. We assign to each rank r a value $h(r, p) = \text{rank}2nb(p - r, p)$ for r even, and $h(r, p) = \text{rank}2nb(r, p)$ for r odd. The only exception is $h(0, p) = 0$. Then, we assign to each rank r a value $v(r, p) = h(r, p) \oplus (h(r, p) \gg 1)$, with \gg being the logical right shift. When clear from the context, we omit p .

3.2.2 Determining the Communication Partner. We describe the tree rooted at rank 0. For trees rooted at any other rank t , rank identifiers are rotated to the right by t positions. The communication partner of a rank r at step j is the rank q such that $v(q) = v(r) \oplus 2^j$ (i.e., a rank that differs in the j -th bit in the v representation). A rank communicates only after it receives the data from its parent. This happens at step i , where i is the position of the highest set bit in $v(r)$. In the example in the right part of Fig. 6, rank 2 receives the data from its parent at step 1, since the most significant bit set to 1 in $v(2) = 011$ is in position 1. Then, at step 2, it sends the data to a rank q such that $v(q) = 011 \oplus 2^2 = 011 \oplus 100 = 111$ (i.e., rank 5). In other words, the algorithm operates as the standard binomial tree algorithm, but using $v(r)$ instead of r , thus reducing the modular distance by 33% (see Appendix A).

3.2.3 Determining Ranks in a Subtree. All ranks in a subtree rooted at r have the same $i + 1$ least significant bits in their v representation, where i is the step at which r received the data from its parent. Indeed, after receiving the data at step i , rank r applies XOR on the bits in positions greater than i . This process recurses, and at each step the $i + 1$ least significant bits remain unchanged. E.g., rank 1 receives data at step $i = 0$, and its $i + 1 = 1$ least significant bit in $v(1)$ is set. Consequently, all its descendants are ranks q whose $v(q)$ also have the least significant bit set. Nodes in distance-doubling *Bine* subtrees are not contiguous, which may require transmitting non-contiguous data for some collectives (Sec. 4.3.1).

4 Collectives Design

4.1 Gather

As in standard binomial trees, each rank gathers data from another rank at each step, halving the number of active ranks until only the root remains. We illustrate in Fig. 7, a binomial and a *Bine* gather over eight ranks, both using distance-halving trees. Data is divided into one “block” per rank. Let $[a, b]$ denote the range of blocks a rank holds at any time. When sending, a rank transmits all the blocks it currently has. In a standard binomial gather, if a rank holds k blocks, it always receives the next k blocks: that is, $[b + 1, b + k]$. E.g., at step 1, rank 4 has blocks $[4, 5]$ and receives $[6, 7]$.

In *Bine* trees, however, the range may extend in either direction. A rank holding $[a, b]$ might receive either $[(b + 1) \bmod p, (b + k) \bmod p]$ or $[(a - k) \bmod p, (a - 1) \bmod p]$, extending its buffer upward or downward. For example, at step 1, rank 0 with blocks

$[0, 1]$ receives $[6, 7]$ from rank 7, extending its buffer upward. In general, even ranks start extending downward, odd ranks upward, alternating direction at each step (e.g., rank 0 extends downward at step 0, upward at step 1, and downward again at step 2).

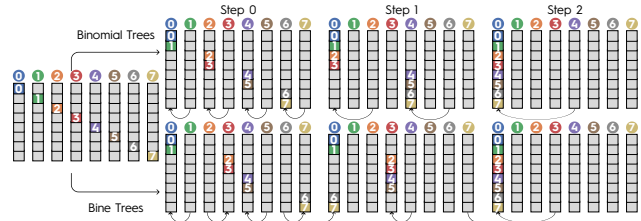


Figure 7: 8-node gather with binomial and *Bine* trees.

4.2 Scatter

For the scatter we can use the opposite process of that used for the gather. In this case, at each step, each rank sends either the bottom or the top half of its remaining buffer $[a, b]$. I.e., if a rank has k blocks of data, it can either send the blocks $[a, (a + \frac{k}{2}) \bmod p]$, or the blocks $[(b - \frac{k}{2}) \bmod p, b]$. For example, since in the gather rank 0 received in the last step the sub-buffer with range $[2, 5]$, then it means that in the scatter it needs to send the sub-buffer with range $[2, 5]$ in the first step. Thus, we need to know what would have been the values of $[a, b]$ in the last step of the gather.

In the gather, even ranks extended their buffer by adding $2^0 + 2^2 + 2^4 + \dots$ to b and subtracting $2^1 + 2^3 + 2^5 + \dots$ from a . Odd ranks did the opposite: they subtracted $2^0 + 2^2 + 2^4 + \dots$ from a and added $2^1 + 2^3 + 2^5 + \dots$ to b . This corresponds to adding or subtracting the binary numbers $0101\dots0101_2$ or $1010\dots1010_2$ to a or b . Thus, it is enough to add and subtract those quantities to the rank identifier r to find the starting $[a, b]$ for the scatter, depending on whether the rank is even or odd. For example, in the first step of the scatter, rank 0 has $[a, b] = [6, 5]$. Then, at each step, either b is decreased by $\frac{k}{2}$ or a is increased by $\frac{k}{2}$, depending on whether the rank is even or odd. This process continues until $k = 1$.

4.3 Reduce-Scatter and Allgather

We discuss in this section the design of the reduce-scatter collective. For the allgather, it is enough to reverse the reduce-scatter communication pattern. We consider a reduce-scatter algorithm based on a vector-halving, distance-doubling butterfly pattern, using the *Bine* butterfly introduced in Sec. 3.1. At each step, each rank exchanges half of its current data with a peer, so the size of the exchanged data halves at each step. Since the communication volume is highest in the early steps, relying on a distance-doubling butterfly helps reduce global traffic. As in standard recursive halving reduce-scatter, each rank sends a total of $n \frac{p-1}{p}$ bytes over $\log_2 p$ steps.

A distance-doubling butterfly reduce-scatter can be conceptually viewed as the concurrent execution of a distance-doubling scatter and a distance-halving reduce. Focusing on the scatter component, unlike the scatter described in Sec. 4.2, a distance-doubling tree is used. While this reduces the volume of inter-group communication, it slightly complicates data selection: a rank r must

send to a rank q all blocks associated with the ranks in the subtree rooted at q . As discussed in Sec. 3.2.3, these subtrees consist of non-contiguous ranks, requiring the exchange of non-contiguous data blocks, which can significantly hinder performance, especially for small- to medium-sized vectors [37].

4.3.1 Dealing with Non-Contiguous Data. To mitigate the performance impact of transmitting non-contiguous data, we consider several possible options. One option is to use MPI datatypes to handle non-contiguous data or to explicitly copy the data to a temporary buffer before every transmission. However, this approach might still introduce a considerable overhead. Instead, for a reduce-scatter, we consider the following alternatives, which we compare in Appendix B:

Block-by-block Each block is transmitted independently. For small and medium-sized vectors, this approach increases the data transmission overhead. At the same time, it creates more opportunities for computation and communication overlap during reduction phases.

Permute Data is first permuted so that subsequent transmissions operate on contiguous regions of memory. This optimization is only applicable when p is a power of two. The permutation is obtained by moving each data block from position i to position $reverse(v(i))$, where $reverse$ denotes the bit-reversal of $v(i)$. As discussed in Sec. 3.2.3, all descendants of a given rank share a fixed number of least significant bits in their v representation. By reversing $v(i)$, the transmitted blocks instead share a fixed number of most significant bits, making them contiguous in memory. For example, in Fig. 8, at step 0 of the reduce-scatter, rank 0 must send all blocks i whose $v(i)$ representation has the least significant bit equal to 1 (see Sec. 3.2.3). That is, it must send blocks 1, 2, 5, and 6. After applying the permutation that places each block i at position $reverse(v(i))$, these four blocks occupy positions 4–7, enabling contiguous transmission.

Send Another option is to skip the permutation and let ranks transmit contiguous data as if the permutation had already been applied. In the example shown in Fig. 8, this means that, in the first step, rank 0 would send the last four blocks of the vector (i.e., 4, 5, 6, and 7 instead of 1, 6, 2, and 5). As a result, at the end of the collective, each rank would hold the block belonging to another rank. For instance, after the reduce-scatter, rank 1 would hold block 4 (since block 1 was not moved in position 4). A final communication step can then be used to exchange and reorder the data correctly, with each rank r sending its block to rank $q = reverse(v(r))$. For example, rank 1 would send its block to rank $q = reverse(v(1)) = 4$. It is worth noting that some collectives combine two operations (e.g., an allreduce implemented as a reduce-scatter followed by an allgather). In such cases, even if ranks do not hold the correct blocks after the first phase, the subsequent collective (e.g., the allgather) implicitly reverses the permutation and restores the correct order, thus avoiding the need for this additional communication step.

Two Transmissions A final option is to perform the reduce-scatter using a distance-halving rather than a distance-doubling butterfly. While this increases traffic over globally oversubscribed links, it simplifies handling non-contiguous data. Specifically, similar to the distance-halving scatter (Sec. 4.2), blocks are contiguous if the buffer is considered circular: any overflow at the end wraps

around to the beginning. Thus, in practice this may require sending two segments: one at the end of the buffer and one at the beginning (for example, see rank 0’s buffer at step 1 of the *Bine* tree in Fig. 7).

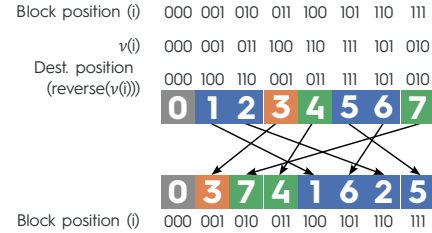


Figure 8: Permutation of non-contiguous data blocks to guarantee contiguous transmissions.

For an allgather, we have a symmetric scenario, i.e., in the *permutate* case, the permutation is done at the end, after all the ranks received the entire buffer, and in the *send* case, the transmission to reorder the blocks is done before the actual steps of the collective operation.

4.4 Allreduce and Alltoall

For the allreduce, we use two algorithms: one for small and one for large vectors. As for standard binomial tree algorithms, the former performs fewer steps, whereas the latter performs more steps but transfers less data. For small vectors, we employ a standard recursive doubling allreduce using *Bine* butterflies. For large vectors, we perform a *Bine* reduce-scatter followed by a *Bine* allgather. Both algorithms create a communication pattern similar to the Swing algorithm [17]. However, unlike Swing, which always sends non-contiguous data [16] and needs to issue multiple sends at each step, *Bine* sends contiguous data (when p is a power of two), leading to $2\times$ performance improvements (see Sec. 5.2.2).

Conceptually, the alltoall can be viewed as a small vector allreduce, where ranks send at each step $n/2$ bytes, and the received data is concatenated with their own rather than being aggregated. At each step, each rank moves the data it wants to keep to the left of its buffer and the data it needs to send to the right, similar to the rotations in Bruck’s algorithm. Each rank tracks the block stored in each buffer position. At the end of the algorithm, a final permutation step is needed to put the data in the correct order.

4.5 Reduce and Broadcast

For *Bine* reduce and broadcast, we propose algorithms for both small and large vectors. The small vector algorithm uses distance-halving *Bine* trees for broadcasting data from the root to the leaves or reducing data from the leaves to the root. For large vectors, we implement the reduce as a reduce-scatter followed by a gather, and the broadcast as a scatter followed by an allgather. The reduce uses a distance-doubling *Bine* butterfly for the reduce-scatter and a distance-halving *Bine* tree for the gather. Data is transmitted contiguously, without the need for reordering, as the gather inverts the block permutation done by the reduce-scatter, placing the blocks back in the correct order. Similarly, the broadcast relies on distance-doubling scatter and distance-halving allgather.

5 Experimental Evaluation

We evaluate *Bine* trees on four supercomputers ranked among the top 11 in the Top500 list at the time of writing. Table 2 summarizes their network topologies and the MPI libraries used, as recommended by their respective supercomputing centers. Additional system-specific details appear in later sections. Our selection covers all four commonly used oversubscribed network topologies, providing a broad and representative evaluation.

Table 2: Systems used in the experimental evaluation. Top500 rankings taken from November 2024 list.

System (Top500 Rank)	Topology	MPI Library
LUMI (#8)	Dragonfly	Cray MPICH v8.1.29
Leonardo (#9)	Dragonfly+	Open MPI v4.1.6
MareNostrum 5 (#11)	2:1 Oversubscribed Fat Tree	Open MPI v4.1.5
Fugaku (#6)	6D Torus	Fujitsu MPI v4.0.1

Implementation. We implemented all *Bine* algorithms from Sec. 4 on top of MPI, without modifying any MPI library. This choice was motivated by both portability (our target systems rely on four different MPI libraries, see Table 2) and fairness, allowing for direct comparison against state-of-the-art algorithms using the same MPI backend. To validate this design choice, we implemented *Bine* versions of allreduce, allgather, and reduce-scatter within Open MPI and compared them to their counterparts built on top of MPI. The observed performance difference was below 3%. Therefore, in the following, we report results using the *Bine* implementations built on top of MPI. This was not the case on Fugaku, where, to concurrently use all the available NICs, our implementation uses the low-level uTofu library [24] (see Sec. 5.4). We implemented all *Bine* algorithms in the PICO benchmarking framework [51, 53], which streamlines comparison with the collective algorithms provided by default in Open MPI and MPICH. Additionally, we provide self-contained reference implementations [50].

Algorithms Used in the Comparison. We compare *Bine* trees against all the collective algorithms available in the MPI implementations on each system. To ensure a fair comparison, we evaluate *Bine* both against the default algorithm selected by MPI and each available algorithm individually, by manually enforcing the selection. We also added other state-of-the-art algorithms from other MPI libraries or versions, such as the *sparbit* allgather algorithm [37, 46] (not available on Open MPI v4.1.x), and the ring-based allreduce algorithm (not available in MPICH 3.4a2, on which Cray MPICH v8.1.29 is based [47]). Moreover, we implemented the Swing algorithm [17] for allgather, reduce-scatter, and allreduce, and the torus-optimized Bucket algorithm [8, 32] (essentially a multi-dimensional ring) for the same collectives. For each system, we begin with a focused comparison of *Bine* and binomial trees, and then extend the evaluation to include all available algorithms.

Benchmarking Methodology. For each collective, we measured performance across different node counts (without requesting any specific node placement) and vector sizes ranging from 32 B to 512 MiB. Due to space constraints, we report results only for power-of-two node counts. Results for non-power-of-two cases are consistent

with those shown and are available in the reproducibility package. All collectives operate on vectors of 32-bit integers. For each combination of node count and vector size, we executed each collective up to 20,000 times for small vectors and five times for 512 MiB vectors. Most experiments were conducted with one process per node; performance with multiple processes per node is discussed in Sec. 6. All vectors are located in host memory except for the experiments in Sec. 6 where we analyze multi-GPU collectives. We followed standard benchmarking practices [29], by discarding the first 20% of iterations as warm-up, and reporting for each iteration the maximum runtime across all ranks.

5.1 Evaluation on LUMI

LUMI [22] relies on a 24-group Slingshot 11 Dragonfly network [19], with 124 nodes per group. We used the LUMI-G partition, where each node has a 64-core AMD EPYC™ Trento 7A53 CPU (organized into four NUMA domains with 128GB of DDR4 memory each), four 200Gb/s Cassini-1 NICs, and four AMD MI250x GPUs.

5.1.1 Comparison with Binomial Trees. We compare *Bine* and binomial trees in terms of both performance and the reduction in the number of bytes transmitted over global links. To assess this, we calculated the total bytes exchanged between ranks. By using the node locations from the `/etc/cray/xname` file, we identified the group each node belongs to and quantified the traffic forwarded between ranks assigned to different groups.

On LUMI, we conducted experiments using between 16 and 1,024 nodes (the maximum allowed) spanning from one to 21 groups. As discussed in Sec. 4.3, *Bine*'s reduce-scatter and allreduce algorithms may send multiple non-contiguous data blocks, rather than a single bulk transfer. This design improves the overlap between communication and computation in reduce-scatter. In contrast, the standard MPICH binomial tree and butterfly implementations transmit large contiguous blocks, without exploiting such overlap. To ensure a fair comparison focused on algorithmic structure rather than implementation-level optimizations, we excluded these *Bine* variants from the analysis. For the alltoall collective, we compared *Bine* with Bruck's algorithm, as it is the closest to binomial algorithms, performing a number of steps logarithmic in p .

Given the large volume of data collected, across eight collectives, up to ten algorithms per collective, nine vector sizes, and up to seven node counts, for a total of over 5,000 configurations, we present a summarized analysis in Table 3⁴. For each collective, we report the fraction of configurations (i.e., combinations of node count and vector size) in which *Bine* outperforms binomial trees and vice versa ("*%Win/%Loss*"). When *Bine* is superior, we report both the average and maximum performance improvements over all the configurations. We compute the average using the geometric mean, which is more appropriate for summarizing ratios [29]. Similarly, when binomial trees outperform *Bine*, we report the corresponding average and maximum performance degradations.

Lastly, we report both the average and maximum reduction in global-link traffic. Here, global links refer to those connecting switches in different Dragonfly groups. We assume packets traverse inter-group connections via minimal paths, an assumption that may

⁴The complete set of detailed results is available in the reproducibility package.

not always hold in practice, especially in low-diameter networks such as Dragonfly [19]. As a result, the reductions we report should be interpreted as lower bounds; the traffic savings induced by *Bine* trees could be even greater than our estimation.

Table 3: Comparison with Binomial Trees on LUMI

Coll.	% Win	Avg/Max Perf. Gain	% Loss	Avg/Max Perf. Drop	Avg/Max Traffic Red.
Allreduce	67%	7%/67%	14%	9%/13%	11%/20%
Allgather	47%	19%/177%	41%	11%/17%	11%/20%
Red.-Scat.	39%	21%/143%	29%	13%/29%	11%/20%
Alltoall	94%	33%/191%	2%	16%/16%	15%/20%
Bcast	67%	25%/79%	27%	16%/29%	88%/94%
Reduce	87%	7%/32%	5%	10%/14%	10%/19%
Gather	71%	13%/47%	16%	13%/32%	9%/25%
Scatter	61%	7%/30%	24%	9%/20%	9%/25%

Overall, *Bine* outperforms standard binomial trees in more than 60% of the configurations on most collectives. The only exceptions are reduce-scatter and allgather, where *Bine* still performs better more often than it is outperformed by binomial trees. For allgather, *Bine* is superior in 47% of the cases, while binomial trees outperform it in 41%, with the remaining 12% showing minimal differences (below 1%). The smaller advantage for these two collectives is due to the additional data permutation step required by *Bine* trees, either through local buffer shuffling or additional data communication (as discussed in Sec. 4.3). However, when *Bine* outperforms binomial trees, the average performance gain is around 20%, with a maximum improvement of up to 177%.

Notably, for alltoall, *Bine* outperforms Bruck’s algorithm in 94% of the cases. Given that alltoall typically involves large data transfers, reducing the traffic on global links becomes especially important. However, as we will discuss in Sec. 5.1.2, logarithmic alltoall algorithms like Bruck’s and *Bine* are typically only effective for small messages and large node count, while linear algorithms tend to perform better in the other cases. It is worth remarking that, as is typical for collective operations, the optimal algorithm depends on both the vector size and the number of nodes. As a result, no single algorithm consistently outperforms the others across all scenarios, and such trade-offs are therefore expected for all collectives.

Bine reduces traffic on global links by an average of 10% across all collectives, and up to 20% at larger node counts, as more nodes lead to higher utilization of global links. The largest reduction, up to 94%, is observed in broadcast. This is due to MPICH (and Open MPI, as shown later) using a large-vector broadcast based on a distance-halving scatter, followed by a distance-doubling allgather [45, 49]. In contrast, *Bine* trees reverse this process, significantly reducing traffic on global links, particularly in the allgather phase.

5.1.2 Comparison with Other State-of-the-Art Algorithms.

To provide a complete comparison, we now compare *Bine* with state-of-the-art algorithms (including binomial trees as well).

Allreduce. We present a detailed analysis of the allreduce in Fig. 9a, using a heatmap to display all combinations of node count and vector size. Each cell either indicates the best-performing algorithm with a single letter or, if *Bine* is superior, shows the performance ratio between *Bine* and the best state-of-the-art algorithm. *Bine* outperforms other algorithms in almost all configurations, with



(a) Allreduce

(b) All collectives

Figure 9: Comparison with state-of-the-art algorithms on LUMI. (a): Each cell shows a letter indicating the best-performing algorithm (N = binomial, D = default), or, when *Bine* is best, the performance ratio between *Bine* and the next-best algorithm. (b): For each collective, the number below the name indicates the percentage of tests where *Bine* outperforms binomial trees. Box plots summarize the distribution of performance improvements in those cases.

peak performance gains of up to 1.62× on medium-sized vectors and high node counts.

Other Collectives. For the remaining collectives, we summarize the corresponding heatmaps using boxplots in Fig. 9b, retaining only the configurations where *Bine* outperforms all other algorithms. Below each collective name, we report the percentage of such cases. For reduce-scatter, we observe up to 65% performance improvements for medium-sized vectors. As discussed in Sec. 4.3 reduce-scatter either sends non-contiguous blocks or permutes the buffer and sends contiguous blocks. At large node counts, permuting the vector for contiguous data results in a 20% performance drop for *Bine* compared to binomial trees, as discussed in Sec. 5.1.1.

For allgather, *Bine* was outperformed by the default Cray MPICH algorithm in 17% of the cases. According to the Cray MPICH manual, the default algorithm leverages architecture-specific optimizations, which we suppose may include, for example, triggered operations. By disabling such optimizations, *Bine* outperformed the state of the art in an additional 18% of cases, with maximum performance gains reaching 89%. A similar trend was observed for broadcast, with *Bine* becoming the top-performing algorithm in 63% of cases when disabling architecture-specific optimizations. For alltoall, *Bine* is the best algorithm in 21% of cases. On 512 and 1,024 nodes with 128 KiB vectors, it outperforms all others by up to 78%. Like Bruck’s algorithm, *Bine* is optimized for small vectors, favoring fewer communication steps at the cost of more data per step. Hence, it performs best at larger scales and with smaller vectors.

5.2 Evaluation on Leonardo

Leonardo [62] uses a Dragonfly+ network topology based on Infiniband HDR. It consists of 23 groups, each containing 180 nodes, organized as two-level fat trees. We used the *Booster* partition, where each node is equipped with two 200 Gb/s dual-port NVIDIA Connect-X6 NICs, a single-socket 32-core Intel Xeon®8358 processor, 512 GB of host memory, and four NVIDIA A100 GPUs.

Table 4: Comparison with Binomial Trees on Leonardo

Coll.	% Win	Avg/Max Perf. Gain	% Loss	Avg/Max Perf. Drop	Avg/Max Traffic Red.
Allreduce	67%	11%/46%	20%	10%/13%	19%/26%
Allgather	91%	9%/54%	0%	0%/0%	19%/26%
Red.-Scat.	71%	4%/12%	14%	6%/6%	17%/23%
Alltoall	79%	25%/70%	0%	0%/0%	15%/15%
Bcast	94%	41%/148%	0%	0%/0%	89%/92%
Reduce	44%	43%/72%	33%	7%/9%	13%/19%
Gather	93%	23%/71%	7%	12%/12%	12%/20%
Scatter	93%	22%/63%	0%	0%/0%	12%/20%

5.2.1 Comparison with Binomial Trees. Table 4 compares *Bine* to binomial trees on configurations from 16 to 2,048 nodes, spanning 3 to 20 groups. Since standard users on Leonardo are limited to jobs of at most 256 nodes, the experiments on 512, 1,024, and 2,048 nodes were conducted during a maintenance window, with support from CINECA, on an otherwise idle system. To reduce the test duration and minimize impact on system operations, we collected data for only allreduce and allgather on jobs larger than 256 nodes.

The results show that *Bine* outperforms binomial trees in most scenarios. For half of the collectives, *Bine* is the best-performing algorithm in over 90% of the cases and matches the performance of binomial trees in the remaining ones. On broadcast we see higher advantages than on LUMI, especially for vectors smaller than 128 KiB, where performance gain where of 4% on LUMI but of 42% on Leonardo. This can be attributed to MPICH relying on distance-halving broadcast [48], whereas Open MPI relies on distance-doubling broadcast [43, 44], which increases the number of bytes transmitted over global links, as we shown in Fig. 1.

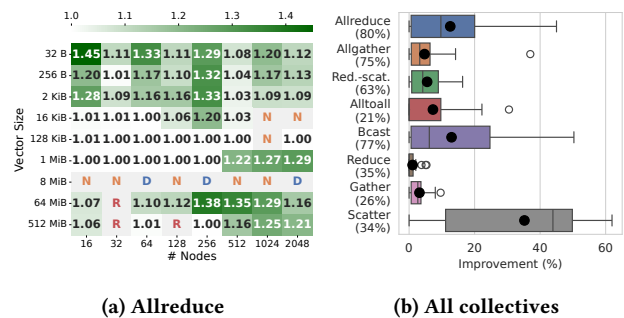
5.2.2 Comparison with Other State-of-the-Art Algorithms.

Allreduce. We compare allreduce performance with state-of-the-art algorithms in Fig. 10a. *Bine* emerges as the best-performing algorithm in 67% of the configurations, achieving performance improvements of up to 1.45 \times . For large vectors at small node counts, the ring algorithm is usually more effective. We verified that part of *Bine*'s performance gains can be attributed to its use of segmentation during allreduce, which enables better overlap between communication and computation. To isolate segmentation effects, we implemented a version of *Bine* allreduce without segmentation.

Without segmentation, the ring algorithm outperforms *Bine* for 512 MiB messages on 256 and 512 nodes. This is expected, as the ring algorithm inherently splits the data into smaller chunks than both *Bine* and butterfly algorithms, which enhances overlap. To have a fair comparison with the ring algorithm, we present *Bine*'s results with segmentation enabled. Still, except for these two cases, *Bine* outperforms all other algorithms even without segmentation.

Other Collectives. We summarize the results in Fig. 10b. For allgather on 2,048 nodes, vectors smaller than 64 MiB benefit from the remapping approach described in Sec.4.4, achieving 2 \times performance improvements compared to algorithms like *Swing* [17] or *sparbit* [37, 46], which send non-contiguous data and introduce significant overhead. For reduce-scatter, *Bine* is the top-performing algorithm in 63% of the cases. For alltoall, results are similar to those on LUMI, with *Bine* being the best algorithm on small vectors.

Finally, *Bine* achieves higher performance on broadcast compared to LUMI, consistently with our findings in Sec. 5.2.1.


Figure 10: Comparison with state-of-the-art algorithms on Leonardo (N = binomial, D = default, R = ring).

5.3 Evaluation on MareNostrum 5

MareNostrum 5 [7] uses a 2:1 oversubscribed fat-tree network topology based on InfiniBand NDR200. Each full-bandwidth sub-tree consists of 160 nodes. We utilized the ACC partition, where each node is equipped with 2 \times Intel Sapphire Rapids 8460Y+ CPUs, 512 GB of DDR5 memory, and four 200 Gb/s NICs. Additionally, each node has 4x Nvidia Hopper GPUs with 64 GB of HBM2 memory.

5.3.1 Comparison with Binomial Trees. We ran experiments from 4 to 64 nodes (the maximum allowed), spanning between one and eight subtrees. We report the results of our analysis in Table 5. Consistent with our findings on LUMI and Leonardo, *Bine* trees outperform binomial tree algorithms in most cases, with performance improvements of up to 158%. However, in a few cases (more evident for gather and scatter), *Bine* increases (on average) the traffic on global links compared to binomial trees. We observed this mostly for small node count, consistently with what we discussed in Sec. 2.

Table 5: Comparison with Binomial Trees on MareNostrum 5

Coll.	% Win	Avg/Max Perf. Gain	% Loss	Avg/Max Perf. Drop	Avg/Max Traffic Red.
Allreduce	80%	9%/46%	2%	6%/6%	2%/11%
Allgather	55%	10%/42%	24%	12%/17%	0%/11%
Red.-Scat.	74%	15%/78%	2%	6%/6%	0%/11%
Alltoall	88%	26%/62%	10%	11%/12%	19%/33%
Bcast	98%	32%/158%	0%	0%/0%	49%/86%
Reduce	51%	31%/80%	22%	19%/40%	2%/7%
Gather	69%	25%/76%	2%	8%/8%	-8%/18%
Scatter	95%	36%/140%	5%	7%/8%	-8%/18%

5.3.2 Comparison with Other State-of-the-Art Algorithms. Fig. 11a summarizes the comparison between *Bine* and the best state-of-the-art algorithms. The results are consistent with our observations on the other platforms. For alltoall, gather, and scatter, *Bine* is the best-performing algorithm in fewer cases. This is primarily due to the smaller scale of the experiments (up to 64 nodes), compared to 1,024 or 256 nodes on LUMI and Leonardo. At these scales, linear algorithms often outperform logarithmic ones, especially for large vectors. Conversely, for vectors smaller than 1 MiB, *Bine* outperformed the other algorithms by up to 2 \times on 64 nodes.

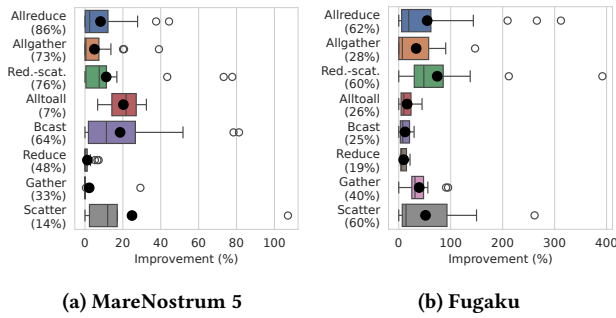


Figure 11: Comparison with state-of-the-art algorithms.

5.4 Evaluation on Fugaku

Fugaku [54] is based on the Tofu Interconnect D [3] and uses a 6D toroidal network. In practice, each job can be allocated a 3D sub-torus. The system is composed of almost 159,000 nodes, each equipped with a Fujitsu A64FX CPU, 32 GiB of HBM memory, and six TNIs (i.e., NICs), each capable of injecting 54.4 Gb/s.

5.4.1 Bine Optimization for Torus Networks. So far, we have not made any assumptions about the network topology. However, we can extend *Bine* trees to better exploit communication locality on torus networks. Instead of considering a flat rank space, we treat ranks as coordinates in a multidimensional space, reducing distance between communicating ranks, as typical in algorithms optimized for toroidal networks [17, 32]. Since each node has six NICs, we divide the vector used in the collective into six parts. Then, we execute six collectives in parallel, each operating on a different part of the vector, using a separate NIC, and transmitting in a different direction of the 6D torus. To ensure that each collective uses a different NIC, we implemented the *Bine* algorithms directly on top of the low-level uTofu library [24]. We provide a more detailed description of the design and the implementation of *Bine* trees for toroidal networks in Appendix D.

5.4.2 Comparison with Binomial Trees. When comparing *Bine* to binomial trees, we observed up to 40× speedups. However, this is largely because these binomial algorithms, based on Open MPI, on which Fujitsu MPI is based, are not optimized for toroidal networks.

5.4.3 Comparison with Other State-of-the-Art Algorithms. As with other systems, we compare both with the default algorithm selected by Fujitsu MPI and with all other available algorithms by explicitly forcing their selection. We performed our analysis on 2×2×2, 4×4×4, 8×8×8, 64×64, and 32×256 nodes jobs. We report results in Fig. 11b. For allreduce, *Bine* trees outperformed state-of-the-art algorithms in 62% of cases, especially for vectors larger than 2 KiB. The highest gains—up to 4.12×—were seen for 128 KiB–64 MiB vectors on 8,192 (32×256) nodes. While Fugaku uses the torus-optimized Trinaryx algorithm [3, 25, 31], which builds three edge-disjoint spanning trees, its linear number of steps limits scalability compared to *Bine*’s logarithmic approach.

For allreduce, reduce-scatter, and scatter, *Bine* trees were the top-performing algorithm in over 60% of the tests, with performance gains of up to 5× for reduce-scatter. In contrast, for broadcast

and reduce, Fujitsu MPI includes algorithms that are optimal on multiported torus networks, leaving little room for improvement. Nonetheless, the fact that *Bine* remains competitive, even against these highly optimized vendor implementations, underscores its strong generalization capability and broad effectiveness.

It is worth noting that Fugaku exhibits the highest performance gains among the four analyzed systems. These gains stem from *Bine*’s ability to reduce traffic on oversubscribed links. In the other three topologies, oversubscription primarily affects global links. In contrast, on a torus, all links can be considered oversubscribed. From another perspective, torus networks have the lowest bisection bandwidth among the topologies considered, and thus benefit the most from *Bine*’s enhanced locality.

6 Discussion

6.1 Impact of Processes per Node

All experiments in Sec. 5 were conducted with one process per node. To study the impact of multiple processes per node, we ran all collectives on 64 nodes on LUMI with either one or four processes per node (LUMI has four NICs per node). Performance was largely consistent, though in a few cases *Bine* achieved larger gains with four processes per node; for example, the 1 MiB reduce-scatter gain increased from 59% to 84%. This is likely due to the higher traffic generated by each node when using multiple processes, which better highlights *Bine*’s global traffic reduction benefits. We observed similar trends on Leonardo and MareNostrum 5.

6.2 Multi-GPU Evaluation

We implemented a GPU-aware version of the *Bine* allreduce algorithm on top of MPI. This was motivated by two main goals. First, it allows us to evaluate the performance of *Bine* on multi-GPU systems and directly compare it against NCCL’s algorithms. Second, it enables the evaluation of a hierarchical implementation of *Bine*. We optimized our design and implementation for large vectors (i.e., implementing the allreduce as a reduce-scatter followed by an allgather), and for the MareNostrum 5 and Leonardo architecture.

Each MareNostrum 5 (and Leonardo) node has four GPUs, fully connected to one another. Our hierarchical *Bine* implementation exploits this topology by first performing an intra-node reduce-scatter, where each GPU exchanges data concurrently with the other three GPUs on the same node. Next, an inter-node *Bine* allreduce is executed among ranks with the same GPU local identifier, operating on the buffer segment received during the reduce-scatter phase. Finally, an intra-node allgather reconstructs the complete result, following a similar pattern to the initial reduce-scatter. As for NCCL, vectors are aggregated on the GPUs.

We evaluated *Bine* against both Open MPI and NCCL (v2.20.5 on MareNostrum 5 and v2.22.3 on Leonardo). On MareNostrum 5, NCCL outperforms MPI algorithms in most cases. However, our MPI implementation of *Bine* surpasses NCCL’s best-performing algorithm across all configurations from 16 to 256 GPUs, for vector sizes larger than 4 MiB. On average, *Bine* achieves a 5% improvement, with gains reaching up to 24% on 256 GPUs. On Leonardo, on 512 GPUs *Bine* improves performance by 15% compared to MPI and remains within 7% of NCCL.

7 Related Work

Locality-Aware and Hierarchical Algorithm Several locality-aware, and hierarchical or multi-leader algorithms [9, 10, 28, 60] have been proposed. These algorithms, however, either require knowledge of the underlying topology [60] or make assumptions about the partitioning of ranks across groups [10]. On the other hand, *Bine* trees are as generic as binomial trees and, as shown in Sec. 6, can be effectively integrated into hierarchical algorithms.

Automatic Algorithm Synthesis Some methods aim to automatically determine the optimal collective algorithm based on network topology and collective specifications [13, 57, 64]. However, their complexity increases exponentially as the system scales. For example, computing a solution for 128 nodes can take up to 11 hours [57], and a new solution may need to be recalculated for each allocation, which makes these approaches not practical on shared supercomputers, where users do not have control over allocations.

Topology-Optimized Algorithms Researchers developed collective algorithms tailored to specific network topologies [4, 23, 39]. In contrast, *Bine* trees are versatile and topology-agnostic and consistently enhance performance across a variety of topologies.

8 Conclusions

In this paper, we introduced *Bine* trees, a novel approach to constructing binomial trees that reduces the distance between communicating ranks and, as a result, reduces traffic on global links and improves performance. We designed new algorithms for eight different collective operations, outperforming state-of-the-art algorithms, including traditional binomial trees and topology-specific methods. We observed performance improvements of up to 5× on 8,192 nodes and reductions in global link traffic of up to 33%, highlighting the potential of *Bine* to deliver significant gains in performance and efficiency across different network topologies.

The main strength of *Bine* trees lies in their generality, being as generic as standard binomial trees and not relying on specific assumptions about the underlying network topology or job allocation. This makes it well-suited for large-scale, shared supercomputing environments. In conclusion, thanks to their broad applicability and ability to reduce network traffic across global links, *Bine* trees represent a significant step toward more efficient, scalable, and flexible collective algorithms. They can effectively replace binomial trees and butterfly-based approaches, especially at large scales.

Acknowledgments

We thank Daniele Di Bari (CINECA) for support with large-scale tests on Leonardo, Kim McMahon (HPE Cray) for assistance with Cray MPICH collective algorithm selection, Kurt Lust for information on node-to-group mapping on LUMI, and Faveo Hörold (ETH Zürich and RIKEN) for help with preliminary tests on Fugaku. This work is supported by the European Union's Horizon Europe under grant 101175702 (NET4EXA), by Sapienza University Grants ADAGIO and D2QNeT (*Bando per la ricerca di Ateneo* 2023 and 2024), and by the European Research Council (ERC) under the European Union's Horizon 2020 research and innovation program (grant PSAP, No. 101002047). Daniele De Sensi is a member of GNCS-INdAM. The authors used ChatGPT for editing; all ideas, content, and conclusions are their own.

References

- [1] Top 500. 2025. Top 500 List. <https://top500.org/>.
- [2] Dennis Abts, Mike Marty, Philip Wells, Peter Klausler, and Hong Liu. 2010. Energy Proportional Datacenter Networks. In *Proceedings of the International Symposium on Computer Architecture*. 338–347. ISCA'10 June 19–23, 2010, Saint-Malo, France.
- [3] Yuichiro Ajima, Takahiro Kawashima, Takayuki Okamoto, Naoyuki Shida, Kouichi Hirai, Toshiyuki Shimizu, Shinya Hiramoto, Yoshiro Ikeda, Takahide Yoshikawa, Kenji Uchida, and Tomohiro Inoue. 2018. The Tofu Interconnect D. In *2018 IEEE International Conference on Cluster Computing (CLUSTER)*. 646–654. doi:10.1109/CLUSTER.2018.00090
- [4] George Almási, Philip Heidelberger, Charles J. Archer, Xavier Martorell, C. Chris Erway, José E. Moreira, B. Steinmacher-Buraw, and Yili Zheng. 2005. Optimization of MPI Collective Communication on BlueGene/L Systems. In *Proceedings of the 19th Annual International Conference on Supercomputing* (Cambridge, Massachusetts) (ICS '05). Association for Computing Machinery, New York, NY, USA, 253–262. doi:10.1145/1088149.1088183
- [5] Scott Atchley, Christopher Zimmer, John Lange, David Bernholdt, Veronica Mellesse Vergara, Thomas Beck, Michael Brim, Reuben Budiardja, Sunita Chandrasekaran, Markus Eisenbach, Thomas Evans, Matthew Ezell, Nicholas Frontiere, Antigoni Georgiadou, Joe Glenski, Philipp Grete, Steven Hamilton, John Holmen, Axel Huebl, Daniel Jacobson, Wayne Joubert, Kim McMahon, Elia Merzari, Stan Moore, Andrew Myers, Stephen Nichols, Sarp Oral, Thomas Papatheodore, Danny Perez, David M. Rogers, Evan Schneider, Jean-Luc Vay, and P. K. Yeung. 2023. Frontier: Exploring Exascale. In *Proceedings of the International Conference for High Performance Computing, Networking, Storage and Analysis (SC '23)*. Association for Computing Machinery, New York, NY, USA, Article 52, 16 pages. doi:10.1145/3581784.3607089
- [6] Scott Atchley, Christopher Zimmer, John Lange, David Bernholdt, Veronica Mellesse Vergara, Thomas Beck, Michael Brim, Reuben Budiardja, Sunita Chandrasekaran, Markus Eisenbach, Thomas Evans, Matthew Ezell, Nicholas Frontiere, Antigoni Georgiadou, Joe Glenski, Philipp Grete, Steven Hamilton, John Holmen, Axel Huebl, Daniel Jacobson, Wayne Joubert, Kim McMahon, Elia Merzari, Stan Moore, Andrew Myers, Stephen Nichols, Sarp Oral, Thomas Papatheodore, Danny Perez, David M. Rogers, Evan Schneider, Jean-Luc Vay, and P. K. Yeung. 2023. Frontier: Exploring Exascale. In *Proceedings of the International Conference for High Performance Computing, Networking, Storage and Analysis (SC '23)*. Association for Computing Machinery, New York, NY, USA, Article 52, 16 pages. doi:10.1145/3581784.3607089
- [7] Fabio Banchelli, Marta Garcia-Gasulla, Filippo Mantovani, Joan Vinyals, Josep Pocerull, David Vicente, Beatriz Eguzkita, Flavio C. C. Galeazzo, Mario C. Acosta, and Sergi Girona. 2025. Introducing MareNostrum5: A European pre-exascale energy-efficient system designed to serve a broad spectrum of scientific workloads. arXiv:2503.09917 [cs.DC] <https://arxiv.org/abs/2503.09917>
- [8] M. Barnett, R. Littlefield, D.G. Payne, and R. Vandegeijn. 1995. Global Combine Algorithms for 2-D Meshes with Wormhole Routing. *J. Parallel and Distrib. Comput.* 24, 2 (1995), 191–201. doi:10.1006/jpdc.1995.1018
- [9] M. Bayatpour, S. Chakraborty, H. Subramoni, X. Lu, and D. Panda. 2017. Scalable Reduction Collectives with Data Partitioning-based Multi-Leader Design.
- [10] Amanda Bienz, Shreeman Gautam, and Amun Kharel. 2022. A Locality-Aware Bruck Allgather. In *Proceedings of the 29th European MPI Users' Group Meeting* (Chattanooga, TN, USA) (*EuroMPI/USA '22*). Association for Computing Machinery, New York, NY, USA, 18–26. doi:10.1145/3555819.3555825
- [11] Nils Blach, Maciej Besta, Daniele De Sensi, Jens Domke, Hussein Harake, Shigang Li, Patrick Iff, Marek Konieczny, Kartik Lakhotia, Ales Kubicek, Marcel Ferrari, Fabrizio Petrini, and Torsten Hoefler. 2024. A high-performance design, implementation, deployment, and evaluation of the slim fly network. In *Proceedings of the 21st USENIX Symposium on Networked Systems Design and Implementation* (Santa Clara, CA, USA) (*NSDI'24*). USENIX Association, USA, Article 57, 20 pages.
- [12] Tommaso Bonato, Sepehr Abdous, Abdul Kabbani, Ahmad Ghalayini, Nadeen Gebara, Terry Lam, Anup Agarwal, Tiancheng Chen, Zhuolong Yu, Konstantin Taranov, Mahmoud Elhaddad, Daniele De Sensi, Soudeh Ghorbani, and Torsten Hoefler. 2025. Uno: A One-Stop Solution for Inter- and Intra-Data Center Congestion Control and Reliable Connectivity. In *Proceedings of the International Conference for High Performance Computing, Networking, Storage and Analysis (SC'25)*. doi:10.1145/3712285.3759884
- [13] Zixian Cai, Zhengyang Liu, Saeed Maleki, Madanlal Musuvathi, Todd Mytkowicz, Jacob Nelson, and Olli Saarikivi. 2021. Synthesizing Optimal Collective Algorithms. In *Proceedings of the 26th ACM SIGPLAN Symposium on Principles and Practice of Parallel Programming* (Virtual Event, Republic of Korea) (*PPoPP '21*). Association for Computing Machinery, New York, NY, USA, 62–75. doi:10.1145/3437801.3441620
- [14] Sudheer Chunduri, Taylor Groves, Peter Mendygral, Brian Austin, Jacob Balma, Krishna Kandalla, Kalyan Kumar, Glenn Lockwood, Scott Parker, Steven Warren, Nathan Wichmann, and Nicholas Wright. 2019. GPCNeT: designing a benchmark suite for inducing and measuring contention in HPC networks. In *Proceedings of the International Conference for High Performance Computing, Networking, Storage and Analysis* (Denver, Colorado) (*SC '19*). Association for Computing

- Machinery, New York, NY, USA, Article 42, 33 pages. doi:10.1145/3295500.3356215
- [15] CINECA. 2025. Leonardo User Guide. <https://wiki.u-gov.it/confluence/display/SCAIUS/LEONARDO+User+Guide> [Accessed 14-04-2025].
- [16] Daniele De Sensi. 2025. Swing Allreduce Simulator. <https://github.com/HLC-Lab/swing-allreduce-sim/blob/main/sst-elements-library-11.1.0/src/sst/elements/ember/mpi/motifs/emberswingcoll.cc> [Accessed 14-04-2025].
- [17] Daniele De Sensi, Tommaso Bonato, David Saam, and Torsten Hoefer. 2024. Swing: Short-cutting Rings for Higher Bandwidth Allreduce. In *21th USENIX Symposium on Networked Systems Design and Implementation (NSDI 24)*. USENIX Association, Santa Clara, CA.
- [18] Daniele De Sensi, Salvatore Di Girolamo, and Torsten Hoefer. 2019. Mitigating Network Noise on Dragonfly Networks Through Application-aware Routing. In *Proceedings of the International Conference for High Performance Computing, Networking, Storage and Analysis (Denver, Colorado) (SC '19)*. ACM, New York, NY, USA, Article 16, 32 pages. doi:10.1145/3295500.3356196
- [19] Daniele De Sensi, Salvatore Di Girolamo, Kim H. McMahon, Duncan Roweth, and Torsten Hoefer. 2020. An In-Depth Analysis of the Slingshot Interconnect. In *Proceedings of the International Conference for High Performance Computing, Networking, Storage and Analysis (Atlanta, Georgia) (SC '20)*. IEEE Press, Article 35, 14 pages. doi:10.1109/sc41405.2020.00039
- [20] Daniele De Sensi, Lorenzo Pichetti, Flavio Vella, Tiziano De Matteis, Zebin Ren, Luigi Fusco, Matteo Turisini, Daniele Cesarini, Kurt Lust, Animesh Trivedi, Duncan Roweth, Filippo Spiga, Salvatore Di Girolamo, and Torsten Hoefer. 2024. Exploring GPU-to-GPU Communication: Insights into Supercomputer Interconnects. In *Proceedings of the International Conference for High Performance Computing, Networking, Storage and Analysis (SC'24)*. doi:ToAppear
- [21] Dylan Patel, Daniel Nishball, and Jeremie Eliahou Ontiveros. [n. d.]. Multi-Datacenter Training: OpenAI's Ambitious Plan To Beat Google's Infrastructure. <https://semianalysis.com/2024/09/04/multi-datacenter-training-openai/> [Accessed 19-03-2024].
- [22] EuroHPC Joint Undertaking. [n. d.]. LUMI Supercomputer. <https://lumi-supercomputer.eu/> [Accessed 19-03-2024].
- [23] Guangnan Feng, Dezun Dong, and Yutong Lu. 2022. Optimized MPI Collective Algorithms for Dragonfly Topology. In *Proceedings of the 36th ACM International Conference on Supercomputing (Virtual Event) (ICS '22)*. Association for Computing Machinery, New York, NY, USA, Article 14, 11 pages. doi:10.1145/3524059.3532380
- [24] Fujitsu. 2025. Development Studio uTofu User's Guide. <https://software.fujitsu.com/jp/manual/manualfiles/m210007/j2ul2482/02enz003/j2ul-2482-02enz0.pdf>.
- [25] Fujitsu. 2025. Topology Awareness in the Tofu Interconnect Series. <https://nowlab.cse.ohio-state.edu/static/media/workshops/presentations/ExaComm16-Invited-Talk-2-Yuichiro-Ajima.pdf> [Accessed 14-04-2025].
- [26] Gemini Team. 2023. Gemini: A Family of Highly Capable Multimodal Models. *arXiv e-prints*, Article arXiv:2312.11805 (Dec. 2023), arXiv:2312.11805 pages. doi:10.48550/arXiv.2312.11805 arXiv:2312.11805 [cs.CL]
- [27] Richard Graham, Manjunath Gorentla Venkata, Joshua Ladd, Pavel Shamis, Ishai Rabinovitz, Vasily Filipov, and Gilad Shainer. 2011. Cheetah: A Framework for Scalable Hierarchical Collective Operations. In *Proceedings of the 2011 11th IEEE/ACM International Symposium on Cluster, Cloud and Grid Computing (CC-GRID '11)*. IEEE Computer Society, USA, 73–83. doi:10.1109/CCGRID.2011.42
- [28] Mert Hidayetoglu, Simon Garcia de Gonzalo, Elliott Slaughter, Pinku Surana, Wen mei Hwu, William Gropp, and Alex Aiken. 2024. HiCCL: A Hierarchical Collective Communication Library. arXiv:2408.05962 [cs.DC] <https://arxiv.org/abs/2408.05962>
- [29] Torsten Hoefer and Roberto Belli. 2015. Scientific benchmarking of parallel computing systems: twelve ways to tell the masses when reporting performance results. In *Proceedings of the International Conference for High Performance Computing, Networking, Storage and Analysis (Austin, Texas) (SC '15)*. Association for Computing Machinery, New York, NY, USA, Article 73, 12 pages. doi:10.1145/2807591.2807644
- [30] Torsten Hoefer, Tommaso Bonato, Daniele De Sensi, Salvatore Di Girolamo, Shigang Li, Marco Heddes, Jon Belk, Deepak Goel, Miguel Castro, and Steve Scott. 2022. HammingMesh: A Network Topology for Large-Scale Deep Learning. In *Proceedings of the International Conference for High Performance Computing, Networking, Storage and Analysis (SC'22)*. doi:10.1109/sc41404.2022.00016 arXiv:2209.01346
- [31] Nanatsuki Hosono, Masaki Iwasawa, and Junichiro Makino. 2021. *Performance Evaluation of MPI Collective Communication on the Supercomputer Fugaku*. Technical Report. Issue 15. The supercomputer "FUGAKU" is a massively parallel computer, which consists of 158,976 nodes. The performance of MPI collective communication is important to achieve highly effective performance. In this article, we will report the performance evaluation of Alltoall, Alltoallv, and Beast on FUGAKU. We surveyed the effect of algorithms, segment size, and node topology. We will report the results and the optimal setting to achieve high efficiency..
- [32] Nikhil Jain and Yogish Sabharwal. 2010. Optimal Bucket Algorithms for Large MPI Collectives on Torus Interconnects. In *Proceedings of the 24th ACM International Conference on Supercomputing (Tsukuba, Ibaraki, Japan) (ICS '10)*. Association for Computing Machinery, New York, NY, USA, 27–36. doi:10.1145/1810085.1810093
- [33] Krishna Kandalla, Hari Subramoni, Gopal Santhanaraman, Matthew Koop, and Dhableswar K. Panda. 2009. Designing multi-leader-based Allgather algorithms for multi-core clusters. In *2009 IEEE International Symposium on Parallel & Distributed Processing*. 1–8. doi:10.1109/IPDPS.2009.5160896
- [34] Yao Kang, Xin Wang, Neil McGlohn, Misbah Mubarak, Sudheer Chunduri, and Zhiling Lan. 2024. Modeling and Analysis of Application Interference on Dragonfly+. *CoRR* abs/2406.15097 (2024). doi:10.48550/ARXIV.2406.15097 arXiv:2406.15097
- [35] N.T. Karonis, B.R. de Supinski, I. Foster, W. Gropp, E. Lusk, and J. Bresnahan. 2000. Exploiting hierarchy in parallel computer networks to optimize collective operation performance. In *Proceedings 14th International Parallel and Distributed Processing Symposium. IPDPS 2000*. 377–384. doi:10.1109/IPDPS.2000.846009
- [36] John Kim, Wiliam J. Dally, Steve Scott, and Dennis Abts. 2008. Technology-Driven, Highly-Scalable Dragonfly Topology. In *Proceedings of the 35th Annual International Symposium on Computer Architecture (ISCA '08)*. IEEE Computer Society, USA, 77–88. doi:10.1109/ISCA.2008.19
- [37] Wilton Loch and Guilherme Koslovski. 2021. Sparbit: a new logarithmic-cost and data locality-aware MPI Allgather algorithm. In *Anais do XXXIII International Symposium on Computer Architecture and High Performance Computing (Belo Horizonte)*. SBC, Porto Alegre, RS, Brasil, 167–176. <https://sol.sbc.org.br/index.php/sbac-pad/article/view/18656>
- [38] Shouxi Luo, Renyi Wang, and Huanlai Xing. 2024. Efficient inter-datacenter ALLReduce with multiple trees. *IEEE Transactions on Network Science and Engineering* (2024).
- [39] Junchao Ma, Dezun Dong, Cunlu Li, Ke Wu, and Liquan Xiao. 2021. PAARD: Proximity-Aware All-Reduce Communication for Dragonfly Networks. In *2021 IEEE Intl Conf on Parallel & Distributed Processing with Applications, Big Data & Cloud Computing, Sustainable Computing & Communications, Social Computing & Networking (ISPA/BDCloud/SocialCom/SustainCom)*. 255–262. doi:10.1109/ISPA-BDCloud-SocialCom-SustainCom52081.2021.00045
- [40] Teng Ma, Thomas Hault, George Bosilca, and Jack J. Dongarra. 2011. Process Distance-Aware Adaptive MPI Collective Communications. In *2011 IEEE International Conference on Cluster Computing*. 196–204. doi:10.1109/CLUSTER.2011.30
- [41] Meta. [n. d.]. Building Meta's GenAI Infrastructure. <https://engineering.fb.com/2024/03/12/data-center-engineering/building-metas-genai-infrastructure/> [Accessed 19-03-2024].
- [42] Timothy Prickett Morgan. 2025. So Who Is Building That 100,000 GPU Cluster for xAI? <https://www.nextplatform.com/2024/07/30/so-who-is-building-that-100000-gpu-cluster-for-xai/>.
- [43] Open MPI. 2025. Open MPI Binomial Tree Broadcast. https://github.com/openmpi/ompi/blob/13d05225283eb9941bb13e0f17688fe6a96d7e19/ompi/mca/coll/base/coll_base_bcst.c#L333.
- [44] Open MPI. 2025. Open MPI Binomial Tree Construction. https://github.com/openmpi/ompi/blob/13d05225283eb9941bb13e0f17688fe6a96d7e19/ompi/mca/coll/base/coll_base_topo.c#L331.
- [45] Open MPI. 2025. Open MPI Scatter Allgather Broadcast. https://github.com/openmpi/ompi/blob/01da1c4c9cd3588737d0bba9a4111c764eca197d/ompi/mca/coll/base/coll_base_bcst.c#L774.
- [46] Open MPI. 2025. Open MPI Sparbit Allgather. https://github.com/openmpi/ompi/blob/13d05225283eb9941bb13e0f17688fe6a96d7e19/ompi/mca/coll/base/coll_base_allgather.c#L228.
- [47] MPICH. 2025. Allreduce Implementations on v3.4a2. <https://github.com/pmodels/mpich/tree/v3.4a2/src/mpi/coll/allreduce> [Accessed 14-04-2025].
- [48] MPICH. 2025. MPICH Binomial Tree Broadcast. https://github.com/pmodels/mpich/blob/2329c3c5b576487f9d2c79acd0253b15b51b12/src/mpi/coll/bcast/bcast_intra_binomial.c#L13.
- [49] MPICH. 2025. MPICH Binomial Tree Broadcast. https://github.com/pmodels/mpich/blob/2329c3c5b576487f9d2c79acd0253b15b51b12/src/mpi/coll/bcast/bcast_intra_scatter_recursive_doubling_allgather.c.
- [50] HLC Lab Sapienza University of Rome. 2025. Bine Trees Reference Implementation. <https://github.com/HLC-Lab/bine-trees>.
- [51] HLC Lab Sapienza University of Rome. 2025. PICO: Performance Insights for Collective Operations. <https://github.com/HLC-Lab/pico/>.
- [52] OpenAI. 2025. Pre-Training GPT-4.5. <https://www.youtube.com/watch?v=6njZopACRuQ>.
- [53] Saverio Pasqualoni, Lorenzo Piarulli, and Daniele De Sensi. 2025. PICO: Performance Insights for Collective Operations. arXiv:2508.16809 [cs.DC] <https://arxiv.org/abs/2508.16809>
- [54] Mitsuhsisa Sato, Yuetsu Kodama, Miwako Tsuji, and Tesuya Odajima. 2022. Co-Design and System for the Supercomputer "Fugaku". *IEEE Micro* 42, 2 (2022), 26–34. doi:10.1109/MM.2021.3136882
- [55] SchedMD. 2025. sbatch User Guide. <https://slurm.schedmd.com/sbatch.html> [Accessed 14-04-2025].
- [56] SchedMD. 2025. Slurm Topology Guide. <https://slurm.schedmd.com/topology.html> [Accessed 14-04-2025].
- [57] Aashaka Shah, Vijay Chidambaram, Meghan Cowan, Saeed Maleki, Madan Musuvathi, Todd Mytkowicz, Jacob Nelson, Olli Saarikivi, and Rachee Singh. 2022. TACCL: Guiding Collective Algorithm Synthesis using Communication Sketches.

- arXiv:2111.04867 [cs.DC]
- [58] Alexander Shpiner, Zachy Haramaty, Saar Eliad, Vladimir Zdornov, Barak Gafni, and Eitan Zahavi. 2017. Dragonfly+: Low Cost Topology for Scaling Datacenters. In *2017 IEEE 3rd International Workshop on High-Performance Interconnection Networks in the Exascale and Big-Data Era (HiPINEB)*. 1–8. doi:10.1109/HiPINEB.2017.11
 - [59] Staci A. Smith, Clara E. Cromei, David K. Lowenthal, Jens Domke, Nikhil Jain, Jayaraman J. Thiagarajan, and Abhinav Bhatle. 2018. Mitigating Inter-Job Interference Using Adaptive Flow-Aware Routing. In *SC18: International Conference for High Performance Computing, Networking, Storage and Analysis*. 346–360. doi:10.1109/SC.2018.00030
 - [60] H. Subramoni, K. Kandalla, J. Vienne, S. Sur, B. Barth, K. Tomko, R. Mclay, K. Schulz, and D.K. Panda. 2011. Design and Evaluation of Network Topology-/Speed-Aware Broadcast Algorithms for InfiniBand Clusters. In *2011 IEEE International Conference on Cluster Computing*. 317–325. doi:10.1109/CLUSTER.2011.43
 - [61] Jesper Larsson Träff. 2006. Efficient allgather for regular SMP-Clusters. In *Proceedings of the 13th European PVM/MPI User's Group Conference on Recent Advances in Parallel Virtual Machine and Message Passing Interface (Bonn, Germany) (EuroPVM/MPI'06)*. Springer-Verlag, Berlin, Heidelberg, 58–65. doi:10.1007/11846802_16
 - [62] Matteo Turisini, Giorgio Amati, and Mirko Cestari. 2024. LEONARDO: A Pan-European Pre-Exascale Supercomputer for HPC and AI applications. *Journal of Large Scale Research Facilities* 8, A186 (2024). doi:10.17815/jlsrf-8-1861
 - [63] Xin Wang, Yao Kang, and Zhiling Lan. 2025. Preventing Workload Interference with Intelligent Routing and Flexible Job Placement Strategy on Dragonfly System. *ACM Trans. Model. Comput. Simul.* 35, 2, Article 17 (April 2025), 22 pages. doi:10.1145/3706104
 - [64] William Won, Midhilesh Elavazhagan, Sudarshan Srinivasan, Swati Gupta, and Tushar Krishna. 2024. TACOS: Topology-Aware Collective Algorithm Synthesizer for Distributed Machine Learning. doi:10.1109/MICRO61859.2024.00068 arXiv:2304.05301 [cs.DC]
 - [65] Xu Yang, John Jenkins, Misbah Mubarak, Robert B. Ross, and Zhiling Lan. 2016. Watch Out for the Bully! Job Interference Study on Dragonfly Network. In *SC '16: Proceedings of the International Conference for High Performance Computing, Networking, Storage and Analysis*. 750–760. doi:10.1109/SC.2016.63

A Detailed Description of Distance-Doubling Bine Trees

Since we want to preserve the 33% modular distance reduction compared to distance-doubling binomial trees, in distance-doubling *Bine* trees, ranks communicate in the opposite order compared to distance-halving butterflies. Specifically, after receiving data at step i (as described in Sec. 3.2), at each subsequent step $j > i$ a rank r sends data to a rank q determined as:

$$q = \begin{cases} \left(r + \sum_{k=0}^j (-2)^k \right) \bmod p, & \text{if } r \text{ is even,} \\ \left(r - \sum_{k=0}^j (-2)^k \right) \bmod p, & \text{if } r \text{ is odd.} \end{cases} \quad (5)$$

The modular distance between two communicating ranks is thus $\sum_{k=0}^j (-2)^k$, implying a 33% reduction in distance compared to standard distance-doubling trees (for the reasons discussed in Sec. 2.4.1). Note that $\sum_{k=0}^j (-2)^k = \frac{1}{3} - \frac{-2^{j+1}}{3}$ is always odd, meaning that even ranks always communicate directly with odd ranks, and vice versa.

We now analyze when the data sent by the root rank r reaches a given rank q . For simplicity, we consider a broadcast with root $r = 0$, but the same reasoning applies to other collectives and to arbitrary roots $r \neq 0$ (in that case, the tree is simply rotated by r positions). At step j , the root $r = 0$ sends data to rank

$$q = \sum_{k=0}^j (-2)^k \bmod p.$$

q is odd, and when q later forwards the data at some step $c > j$, it sends it to:

$$t = q - \sum_{k=0}^c (-2)^k \bmod p = \sum_{k=0}^j (-2)^k - \sum_{k=0}^c (-2)^k \bmod p.$$

i.e., the sign between each summation alternates from positive to negative and vice-versa.

To generalize, consider the path through which data from root 0 reaches a rank q after h steps $s_0 < s_1 < \dots < s_{h-1}$. If q is odd, since communication alternates between even and odd ranks, h must be odd, and:

$$q = \sum_{i=0}^{s_0} (-2)^i - \sum_{i=0}^{s_1} (-2)^i + \sum_{i=0}^{s_2} (-2)^i - \dots + \sum_{i=0}^{s_{h-1}} (-2)^i \bmod p.$$

Simplifying the summations gives:

$$q = \sum_{i=0}^{s_0} (-2)^i + \sum_{i=s_1+1}^{s_2} (-2)^i + \dots + \sum_{i=s_{h-2}+1}^{s_{h-1}} (-2)^i \bmod p. \quad (6)$$

The right-hand side corresponds to a negabinary representation, whose least significant bit is 1, as illustrated in Fig. 12 for a 12-bit string with $s_0 = 1$, $s_1 = 5$, and $s_2 = 8$.

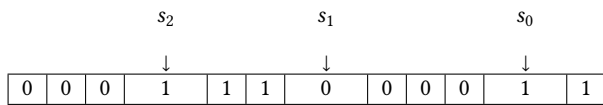


Figure 12: Negabinary representation corresponding to Eq. 6 with $s_0 = 1$, $s_1 = 5$, and $s_2 = 8$.

In this representation, the leftmost and rightmost positions of each contiguous sequence of 1s correspond to the values of the s_i . Thus, if q is odd and its negabinary encoding matches Fig. 12, the data from the root reached q through step $s_0 = 1$, then $s_1 = 5$, and finally $s_2 = 8$.

To isolate the positions of the s_i (i.e., to create a binary string with 1s only at those positions, e.g., 000100100010 for the example just described), we define $h(q, p)$ as the negabinary string in Fig. 12, and compute:

$$v(q, p) = h(q, p) \oplus (h(q, p) \gg 1).$$

In essence, by inspecting the bits of $v(q, p)$, we can reconstruct exactly how the data propagated from the root to rank q .

Rank q receives the data at step s_{h-1} , corresponding to the most significant bit set to 1 in $v(q, p)$. At each subsequent step j , it forwards the data to a rank whose v differs only in bit j —that is, the destination rank has a 1 in position j and 0s in all more significant positions, consistent with the algorithm's design.

The same reasoning extends to even ranks. In that case, h is even, and:

$$q = \sum_{i=0}^{s_0} (-2)^i - \sum_{i=0}^{s_1} (-2)^i + \sum_{i=0}^{s_2} (-2)^i - \dots - \sum_{i=0}^{s_{h-1}} (-2)^i \bmod p,$$

which simplifies to:

$$q = - \sum_{i=s_0+1}^{s_1} (-2)^i - \sum_{i=s_2+1}^{s_3} (-2)^i - \dots - \sum_{i=s_{h-2}+1}^{s_{h-1}} (-2)^i \bmod p.$$

Multiplying both sides by -1 yields:

$$-q = \sum_{i=s_0+1}^{s_1} (-2)^i + \sum_{i=s_2+1}^{s_3} (-2)^i + \dots + \sum_{i=s_{h-2}+1}^{s_{h-1}} (-2)^i \bmod p.$$

Adding p to both sides, we obtain:

$$p - q = \sum_{i=s_0+1}^{s_1} (-2)^i + \sum_{i=s_2+1}^{s_3} (-2)^i + \dots + \sum_{i=s_{h-2}+1}^{s_{h-1}} (-2)^i \bmod p. \quad (7)$$

The right-hand side again represents a negabinary number, but with its least significant bit equal to 0, as shown in Fig. 13 for $s_0 = 1$, $s_1 = 5$, $s_2 = 8$, and $s_3 = 10$. For this reason, for even q we define:

$$v(q, p) = h(p - q, p) \oplus (h(p - q, p) \gg 1).$$

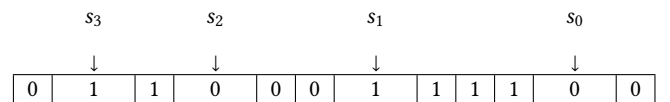


Figure 13: Negabinary representation corresponding to Eq. 7, with $s_0 = 1$, $s_1 = 5$, $s_2 = 8$, and $s_3 = 10$.

B Comparison of Non-Contiguous Data Transfers Techniques

Vector Size	8	16	32	64	128	256	512	1024
32 B	P 0.92x	N/A						
256 B	P 0.92x	P 0.93x	P 0.94x	P 1.01x	N/A	N/A	N/A	N/A
2 KiB	P 0.88x	P 0.93x	P 0.93x	P 1.09x	P 1.02x	P 1.48x	S 0.88x	N/A
16 KiB	P 0.82x	P 0.90x	P 0.90x	P 1.36x	P 1.16x	P 2.27x	S 1.48x	S 3.00x
128 KiB	B 1.32x	B 1.18x	S 0.89x	S 1.06x	P 0.97x	P 1.24x	S 1.19x	B 1.03x
1 MiB	B 1.21x	S 1.01x	S 1.02x	B 1.10x	B 1.03x	B 1.32x	B 1.39x	B 1.27x
8 MiB	B 1.19x	B 1.16x	S 1.07x	T 0.91x	T 0.86x	T 0.93x	T 0.87x	T 0.83x
64 MiB	B 1.14x	B 1.15x	B 1.08x	B 0.93x	B 1.00x	B 0.94x	T 0.86x	B 0.85x
512 MiB	T 1.16x	S 1.16x	S 1.06x	T 0.93x	T 0.91x	T 0.96x	T 0.87x	T 0.87x

Figure 14: Comparison of techniques for handling the transmission of non-contiguous data (see Sec. 4.3.1). Results are obtained on LUMI for an allgather collective operation. Each cell shows a letter corresponding to the best technique (B=Block-by-block, P=Permute, S=Send, T=Two Transmissions), and the performance gain compared to standard binomial butterflies.

In Fig. 14, we compare the different techniques for handling the transmission of non-contiguous data (see Sec. 4.3.1) for an allgather executed on LUMI. Each cell reports the best-performing technique (B=Block-by-block, P=Permute, S=Send, T=Two Transmissions) together with its performance gain relative to standard binomial butterflies. We first observe that, for small vectors, the *permute* technique achieves the highest performance, with gains of up to 2.27x over binomial butterflies. Since the number of blocks, and thus the number of memory copies required for the permutation, grows with the number of nodes, the cost of permutation increases with system scale. As a result, for larger node counts, the *send* technique becomes more effective, as it avoids buffer permutation and instead adds a final communication step to restore the correct order.

For larger vectors, the cost of permutation further increases because more data must be rearranged, making the *block-by-block* technique more efficient. However, as the number of nodes grows, the number of transmissions also rises, and the best-performing approach becomes the *two transmissions* technique. Finally, we note that the current implementation still offers opportunities for optimization. For instance, in the *permute* variant, data permutation could be overlapped with communication by employing an additional buffer, in which data received during the previous step is permuted while data for the current step is transmitted.

C Managing Non-Power of Two Ranks

If the number of ranks is not a power of 2, different strategies can be adopted. The most straightforward approach follows techniques

commonly used in binomial trees [48]. For clarity, consider a one-dimensional torus of size p not equal to a power of two. Let $p' = 2^{\lfloor \log_2 p \rfloor}$. For tree-based collectives (e.g., a broadcast), one option is to first execute the collective among p' ranks, and then have the remaining $p - p'$ ranks receive the data from $p - p'$ of the already-participating ranks.

For butterfly-based collectives (e.g., reduce-scatter), a straightforward solution is to have the last $p - p'$ ranks forward their data to the first $p - p'$ ranks, then execute the reduce-scatter on these p' ranks, and finally redistribute part of the resulting data back to the last $p - p'$ ranks. However, this doubles the total communication volume, since the first $p - p'$ ranks must first receive an entire vector from one of the last ranks before participating in the reduce-scatter.

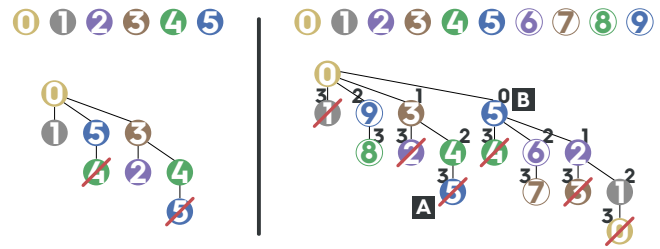


Figure 15: Bine trees constructed for a number of ranks that is not a power of 2.

If p is even, we can adopt a simpler approach that does not increase the total communication volume. In this case, the collective is executed as usual, but some ranks may be reached twice. This situation is illustrated in Fig. 15 for collectives with 6 and 10 nodes. For simplicity, a tree is shown, but the same applies to a butterfly, which, as discussed in Sec. 3.1, can be seen as the superposition of multiple trees, each rooted at a different rank.

For example, in the 6-node case, both rank 4 and rank 5 are reached twice. This would compromise correctness. For instance, in a reduce operation, the same contribution might be applied twice. To avoid this issue, it suffices to remove one of the two subtrees rooted at the rank that is reached twice. For example, for rank 4 we can either remove it as a leaf (and the children of rank 5), or remove the subtree rooted at rank 4 (which has rank 5 as a child).

To determine which of the two subtrees to remove, let us consider the 10-node tree shown in Fig. 15. Each node is annotated with the step at which the data from the root reaches it (e.g., node 8 is reached at step 3, since node 0 sends the data to node 9 at step 2, and then node 9 forwards it to node 8 at step 3). Since the subtree reached later always contains fewer nodes (which are also contained in the other subtree), we discard that one, as removing the larger subtree could compromise correctness. This is evident in the case of node 5. We remove the subtree reached at step 3 (Fig. 15 A), since removing the other one (Fig. 15 B) would disconnect a larger portion of the tree, leaving some nodes unreachable (e.g., nodes 6 and 7).

It is worth noting that this approach cannot be directly applied if p is odd. Since communication always occurs in pairs, some ranks would inevitably attempt to communicate with a rank that is already engaged. In such cases, one must revert to the standard techniques discussed above.

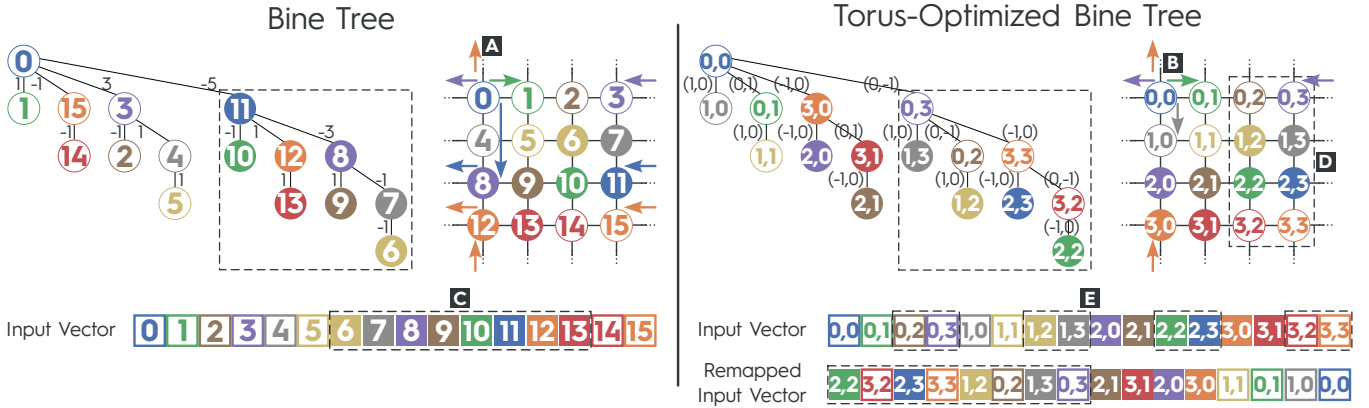


Figure 16: Optimization of a distance-halving *Bine* tree for a 2D torus. For both *Bine* tree and torus-optimized *Bine* tree we show both the 2D torus on which the tree is built, and the corresponding tree.

D Optimization for Torus Networks

We now describe how to extend *Bine* trees to better exploit communication locality on torus networks. For simplicity, we focus on trees; however, as discussed in Sec. 3.1, a butterfly can be viewed as a superposition of multiple trees, each rooted at a different rank. Therefore, the considerations in this section apply to both binomial trees and butterflies. We first assume that each torus dimension is a power of 2, and then generalize to arbitrary dimension sizes.

D.1 Selection of Communicating Partner

We illustrate this in Fig. 16, comparing a standard *Bine* tree with its torus-optimized counterpart on a 4×4 torus. Standard *Bine* trees optimize for modular distance assuming a one-dimensional torus, which does not necessarily yield efficient communication paths in higher-dimensional topologies. For example, in the left part of Fig. 16, edge labels show the modular distance between communicating ranks as if they were arranged on a 1D torus. A sign indicates communication direction: a minus sign denotes communication to the left of the source rank. For instance, the modular distance between ranks 0 and 15 is computed as:

$$d(0, 15) = \min((0-15) \bmod 16, (15-0) \bmod 16) = \min(1, 15) = 1,$$

which we label as -1 since the shorter path wraps leftward. However, on a 2D torus, the actual distance between ranks 0 and 15 is 2 hops (see Fig. 16 A), traversing multiple links and potentially introducing additional congestion, as discussed in Sec. 1.

To address this, we treat ranks as coordinates in a multidimensional space and apply the *Bine* construction dimension by dimension, similar to other torus-optimized algorithms [17, 32]. Communication partners are then chosen along single dimensions: instead of distances $-5, 3, -1, 1$, rank 0 exchanges with ranks at $(0, -1)$, $(-1, 0)$, $(0, 1)$, $(1, 0)$. Concretely, rank 0 at coordinates $(0, 0)$ first communicates with $(0, 3)$ (rank 3), then with $(3, 0)$ (rank 12), then with $(0, 1)$ (rank 1), and finally with $(1, 0)$ (rank 4). As shown in Fig. 16 E, this approach reduces the number of crossed links, alleviating congestion and improving performance.

D.2 Data Handling

However, while this approach reduces communication distance, it complicates data management. To illustrate this issue and possible solutions, we consider a scatter operation implemented with a *Bine* tree. Other collectives are handled similarly; for example, in a gather, data flows from the leaves to the root, and in an allgather, each rank uses its own tree. The root splits the data into “blocks”, one per rank. Each node must forward to its children all the blocks belonging to the subtree rooted at that child. In standard distance-halving *Bine* trees, the descendants of any node are contiguous. For example, in Fig. 16, the subtree rooted at rank 11 (highlighted by the dashed box) contains only consecutive ranks. As a result, when rank 0 sends data to rank 11, it transfers a set of contiguous memory blocks (i.e., the blocks in the range $[6, 13]$ Fig. 16 C).

In contrast, in torus-optimized *Bine* trees the descendants of a node are no longer contiguous, since ranks are arranged according to multidimensional coordinates. Returning to the scatter example, in the first step rank 0 (with coordinates $(0, 0)$) sends data to rank 3 (with coordinates $(0, 3)$). In this case, although those ranks are contiguous in the 2D torus (Fig. 16 D), the blocks in the one-dimensional input vector are not (Fig. 16 E). This increases data-handling complexity compared to the standard case, and can significantly hinder performance, especially for small- to medium-sized vectors [37], as we show in Sec. 5.

An alternative is to permute the vector before transmission, ensuring that all subsequent sends by any rank involve contiguous data. This can be achieved by renumbering the nodes according to a *DFS postorder* traversal (i.e., the order obtained by a depth-first search where a node is visited after all its children). For instance, in Fig. 16, the block originally at position 10 (coordinates $(2, 2)$) is moved to position 0, the block at position 14 (coordinates $(3, 2)$) to position 1, and so forth.

To avoid the initial permutation, ranks could send contiguous data as if the permutation had occurred. At the end of the collective, however, each rank would hold the wrong block; for instance, rank 10 (coordinates $(2, 2)$) would receive the data intended for rank 0 (coordinates $(0, 0)$). This can be corrected by adding an additional communication step at the end, where rank 10 sends its data

to the correct rank (i.e., rank 0), and other ranks perform analogous exchanges.

Finally, some collectives are composed of multiple operations, such as an allreduce implemented as a reduce-scatter followed by an allgather. In these cases, even if the reduce-scatter places blocks in the wrong order, the subsequent allgather, which effectively inverts the reduce-scatter schedule, restores the blocks to the correct order.

D.3 Non-Power of Two

If one (or more) torus dimensions is not a power of 2, we can rely on techniques commonly used in standard binomial trees and butterflies, as discussed in Appendix C. On a multidimensional torus, however, beyond the challenges already mentioned, such techniques complicate the selection of the p' ranks, particularly when trying to preserve short communication distances among participating ranks. As a consequence, several communication steps may require traversing long paths across multiple links.

Moreover, running the collective on a subtorus with p' ranks (whose dimensions are all powers of two) would disrupt the direct correspondence between torus coordinates and linear rank numbering, thereby complicating both process mapping and data management. When all torus dimensions are even, we instead adopt the approach described in Appendix C, which eliminates duplicated subtrees. This strategy, illustrated in Fig. 17 for a 2×6 torus, does not require identifying a subtorus and does not add extra complexity compared to the power-of-two case.

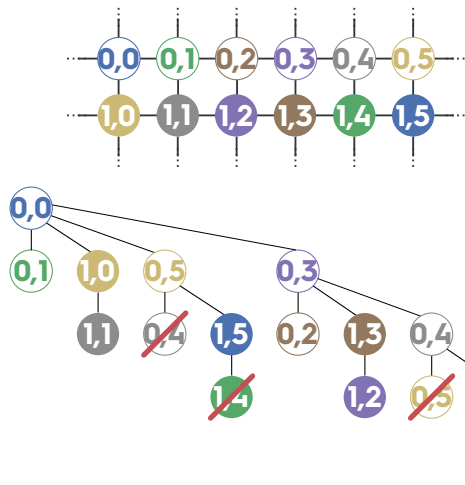


Figure 17: Torus-optimized *Bine* trees for toroidal networks with dimensions that are not powers of 2.

D.4 Multi-ported Torus

On many torus networks, nodes can transmit simultaneously in all directions. For example, on Fugaku each node is equipped with six TNIs (i.e., NICs), each capable of injecting 54.4 Gb/s. To fully exploit this capability, on a D -dimensional torus we divide the vector used in the collective into $2D$ parts. We then execute $2D$ collectives in parallel, each operating on $n/2D$ bytes, using a separate NIC and transmitting in a different direction.

For instance, as shown in Fig. 18 for a $2D$ torus, rank 0 would normally communicate sequentially in the order east (E) \rightarrow north (N) \rightarrow west (W) \rightarrow south (S). With port parallelization, this order is applied only to 1/4 of the data. In parallel, another 1/4 is transmitted in the order N \rightarrow W \rightarrow S \rightarrow E, another 1/4 with order W \rightarrow S \rightarrow E \rightarrow N, and the last 1/4 with order S \rightarrow E \rightarrow N \rightarrow W. In this way, all four NICs are active in parallel, thus saturating the available bandwidth. It is worth remarking that on rectangular torus, after some step some of the ports will not be used anymore, since no more communications will happen along those shorter dimensions.

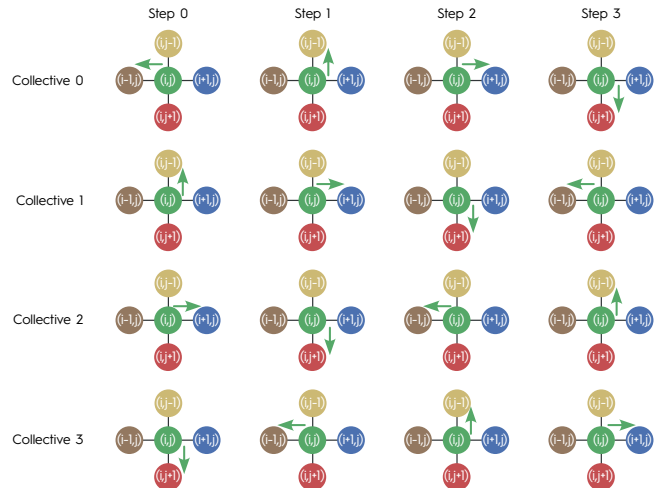


Figure 18: Communications happening on a $2D$ torus when multiported *Bine* tree algorithms are used.

To ensure that each collective uses a different NIC, we implemented the *Bine* algorithms directly on top of the low-level uTofu library, caching registered remote addresses as we suppose it would likely happen in Fujitsu MPI as well. To simplify the management of several interfaces, each one is managed by a separate thread.